remote sensing

MDPI

Review

Soil Moisture Monitoring Method and Data Products: Current Research Status and Future Development Trends

Ruihao Liu [1,2,3], Cun Chang [1,2,3], Ruisen Zhong [1,2,3,*] and Shiyang Lu [1,2]

[1] State Key Laboratory of Ecological Safety and Sustainable Development in Arid Lands, Xinjiang Institute of Ecology and Geography, Chinese Academy of Sciences, Urumqi 830011, China; liuruihao24@mails.ucas.ac.cn (R.L.); changcun@ms.xjb.ac.cn (C.C.); lushiyang24@mails.ucas.ac.cn (S.L.)
[2] University of Chinese Academy of Sciences, Beijing 100049, China
[3] Key Laboratory of GIS & RS Application, Xinjiang Uygur Autonomous Region, Urumqi 830011, China
* Correspondence: zhongrs@ms.xjb.ac.cn

Highlights

What are the main findings?

- Summarizes and analyzes the advantages and limitations of various soil moisture monitoring techniques.
- Compiles and evaluates existing soil moisture datasets, highlighting their respective strengths and weaknesses.

What are the implications of the main findings?

- Provides a systematic and comprehensive structural summary of soil moisture monitoring methods.
- Conducts a trend analysis of the development of major monitoring methods and soil moisture datasets.

Abstract

Soil moisture (SM) is a key variable regulating land–atmosphere energy exchange, hydrological processes, and ecosystem functioning. Though important, there are still unresolved problems in accurate SM monitoring and the practical application and validation of existing methods. In this review, we integrate mechanistic classification and applicability and constraint discussions to develop a coherent understanding of current SM monitoring approaches. Within this framework, in situ measurements, optical and thermal infrared methods, active and passive microwave remote sensing (RS) techniques, and model-based simulations are compared, and publicly accessible SM dataset products are comparatively analyzed in terms of product characteristics and application limitations. Different from other published reviews, this study covers a large scope of SM monitoring methods varying from in situ observation to RS inversion, and classifies them based on their mechanisms, thereby constructing a complete comparative framework for SM research. Moreover, three types of open-access SM dataset products are investigated, optical and microwave RS products, model simulation and data fusion products, and reanalysis dataset products, and evaluated according to their resolution, depth, applicability, advantages, and limitations. By doing so, it is concluded that in situ observations remain essential for calibration and validation but are spatially limited. Optical and thermal infrared methods are restricted by atmospheric conditions and a shallow penetration depth, while microwave techniques exhibit varying performances under different vegetation and soil conditions. Existing datasets differ significantly in resolution, consistency, and coverage, making no single

check for updates

Academic Editor: Dusan Gleich

Received: 22 October 2025
Revised: 22 November 2025
Accepted: 3 December 2025
Published: 5 December 2025

Citation: Liu, R.; Chang, C.; Zhong, R.; Lu, S. Soil Moisture Monitoring Method and Data Products: Current Research Status and Future Development Trends. *Remote Sens.* **2025**, *17*, 3945. https://doi.org/10.3390/rs17243945

Copyright: © 2025 by the authors. Licensee MDPI, Basel, Switzerland. This article is an open access article distributed under the terms and conditions of the Creative Commons Attribution (CC BY) license (https://creativecommons.org/licenses/by/4.0/).

product universally applicable. Future research should focus on multi-source and spatiotemporal data fusions, the integration of machine learning with physical mechanisms, enhancement for cross-sensor consistency, the establishment of standardized uncertainty evaluation frameworks, and the refinement of high-order RTMs and parameterization.

Keywords: soil moisture; in situ observation techniques; optical/microwave remote sensing; physical models; empirical models; SMAP/SMOS satellites; soil moisture datasets

1. Introduction

Soil moisture (SM) is a fundamental component of the terrestrial water cycle, influencing global climate regulation, agricultural productivity, water management, and ecosystem stability [1]. It mediates land–atmosphere exchanges of water and energy, thereby affecting plant growth [2], evapotranspiration, and surface runoff [3]. Consequently, SM data are widely applied in climate change research [4], drought monitoring, irrigation scheduling [5], water resource management [6], flood forecasting [7], and ecological assessments. SM variability is controlled by factors such as surface cover, vapor transport, and temperature, which jointly determine soil infiltration, groundwater recharge, and runoff generation. Accurate and real-time SM monitoring is therefore crucial for understanding climate change impacts, wetland conservation [8], efficient irrigation management [2], disaster prediction [9], and sustainable water use. Moreover, it provides essential data support for hydrological and climatic studies [10,11], ecosystem health evaluation [12], environmental protection, and agricultural development [13,14]. Its accurate monitoring is vital for sustainable agriculture, optimized water use, and studies of climate–ecological processes.

In recent years, SM research has advanced significantly with the development of in situ observation and remote sensing (RS) technologies. In situ methods provide high-precision measurements at small scales [9] but are limited by instrument operability, portability, and cost [15]. RS enables large-scale, multi-temporal inversion, but its accuracy is affected by sensor type, observation conditions, and calibration. Optical techniques offer high spatial resolutions [8] but are sensitive to atmospheric, evapotranspiration (ET), vegetation, and soil conditions [16], whereas microwave techniques are more robust and can penetrate soil but have limited spatial resolutions and are influenced by soil roughness [17]. Multi-source data fusion has emerged to integrate the strengths of different approaches, improving accuracy, spatial coverage, and temporal continuity [18,19]. However, data complexity and environmental variability can limit regional performance. Future research should focus on high-precision, high-resolution inversion, efficient data assimilation and fusion algorithms, predictive and adaptive models [13,20], and novel sensors to enhance accuracy. By combining RS, ground measurements, and data analysis, a comprehensive understanding of SM spatiotemporal dynamics can be achieved, providing critical support for global-scale research and sustainable development.

At the same time, numerous reviews have been conducted, such as some focusing on specific techniques such as the GNSS method [21,22], machine learning models [23,24], or physical mechanisms of active and passive microwave inversion [25], or others diving into certain applications [26]. They generally lack a comprehensive coverage of SM monitoring methods and fail to provide a clear and systematic classification framework. While other reviews touch upon various techniques [27], they primarily emphasize explanation and comparison between features of different SM monitoring methods, omitting reviewing dataset products to guide practical application. In view of these considerations, this paper

aims to provide a comprehensive and systematic synthesis of SM monitoring methods, indices, and models, and provides a critical analysis of their respective advantages and disadvantages in practical applications of recent research trends. In order to achieve these goals, all reviewed methods are categorized into in situ observations, optical RS, thermodynamic and energy balance approaches, and microwave RS, and each category is thoroughly compared and summarized. In addition, a comparison of different public soil moisture datasets is also made, thereby providing a more practical and unified perspective for the research community.

This survey is structured as follows: Section 2 provides a detailed overview of in situ soil moisture observation techniques. RS-based inversion approaches and their underlying principles are explicated in Section 3. Section 4 reviews the characteristics and distinctive features of publicly available datasets generated from active and passive RS observations in combination with reanalysis products. Building upon these foundations, in Section 5, we discuss methodological advances from the perspective of different categories of approaches, with an emphasis on their future directions and applicability.

Figures 1–3 illustrate the keywords, author affiliations, and author citation relationships from the referenced literature in this paper, providing a helpful guide to analyze the research outcomes of different institutions and authors.

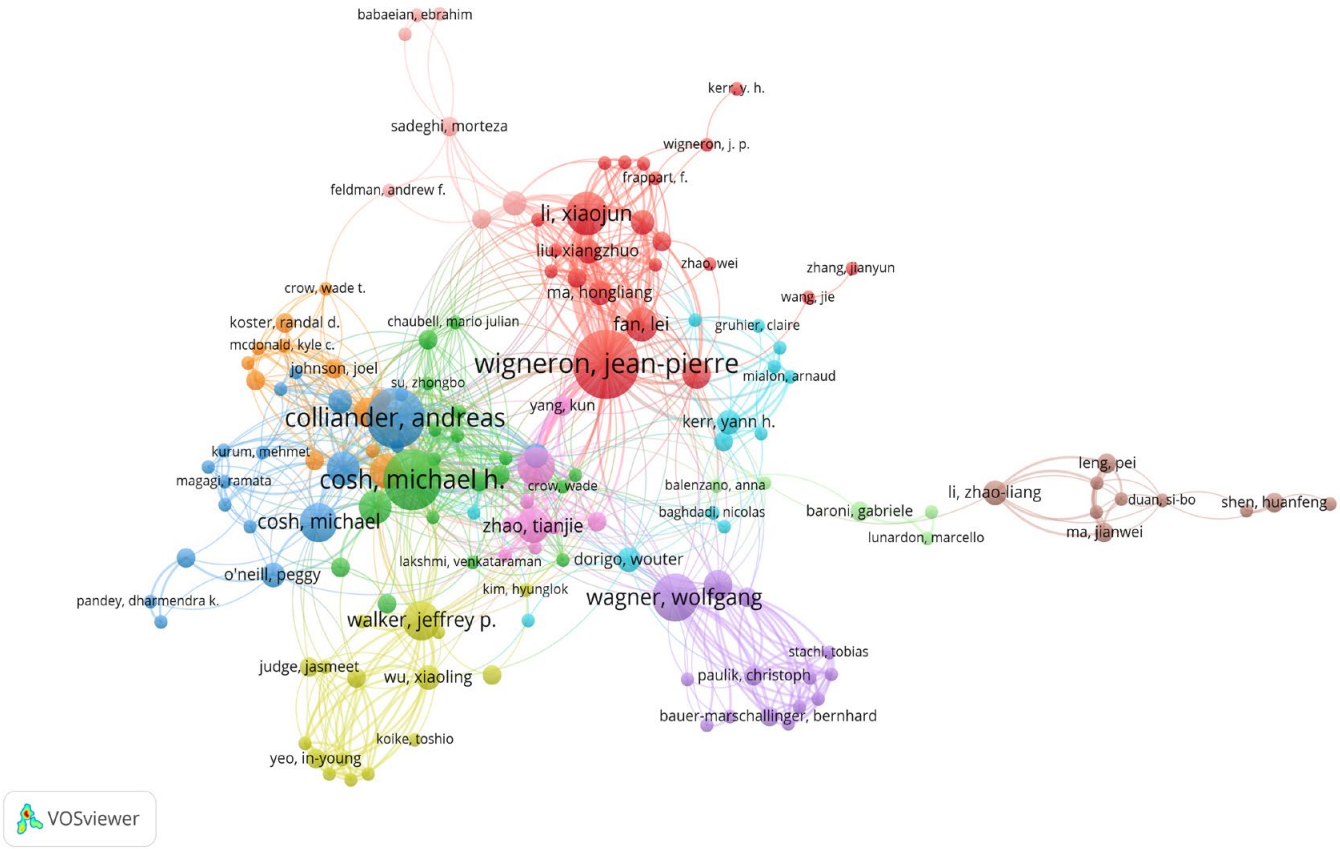


Figure 1. Author co-citation network map cited by this article.

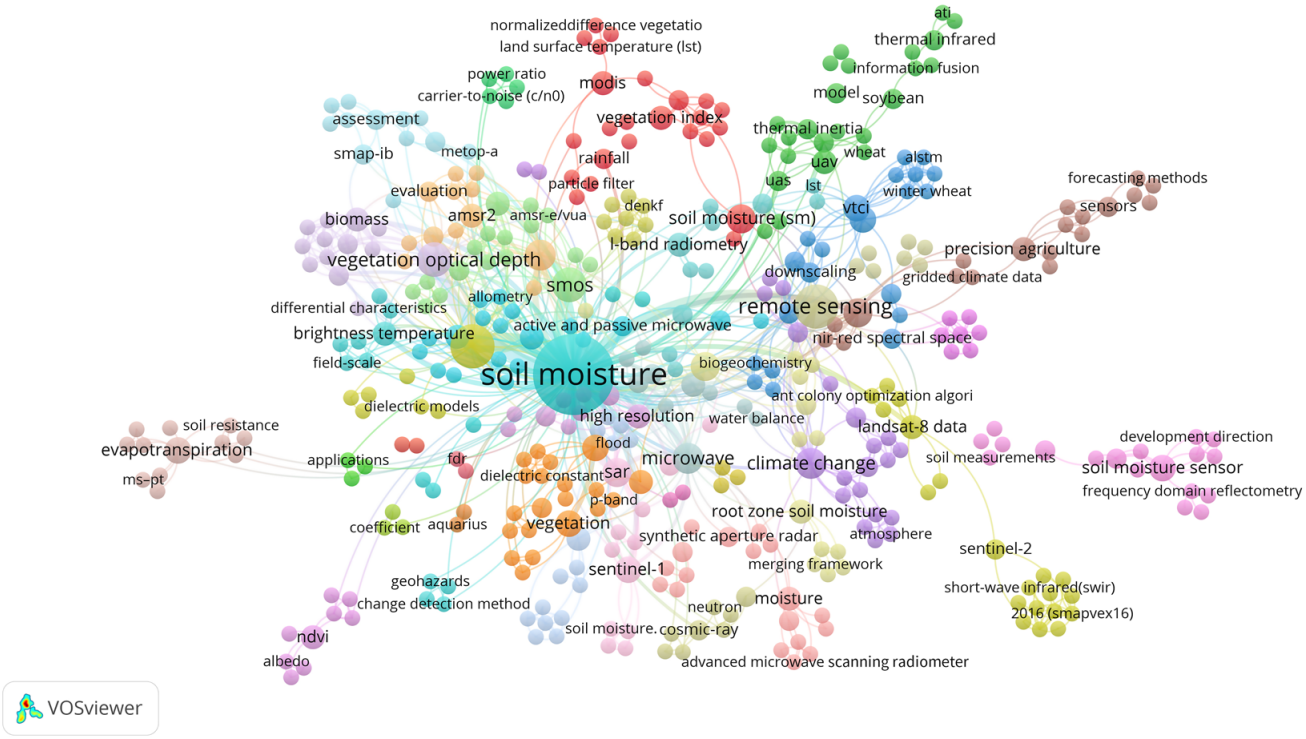


Figure 2. Keyword co-occurrence network map cited by this article.

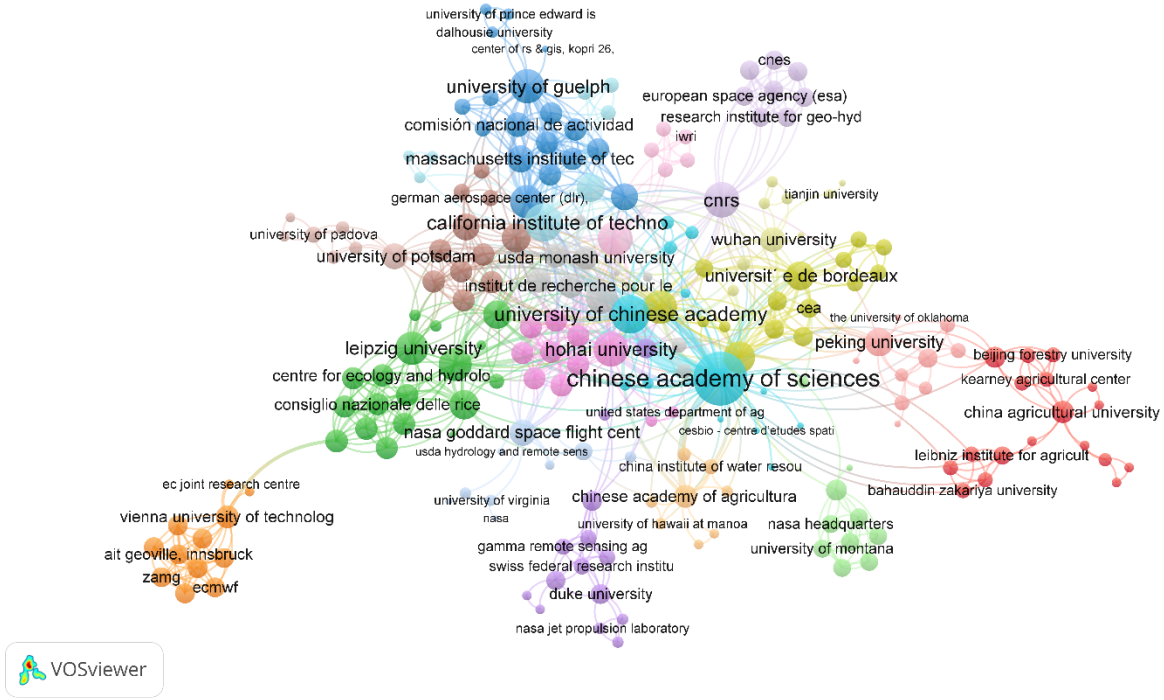


Figure 3. Author–institution collaboration network map cited by this article.

2. In Situ Observation-Based Soil Moisture Monitoring Methods

Soil moisture (SM) monitoring methods based on in situ observation can be categorized into invasive and non-invasive techniques. The choice of method during measurement is often influenced by various factors, including the environment, user expertise, the cost of usage and maintenance, operational complexity, portability, offline availability, and environmental impact [15].

2.1. Invasive Detection Technologies

Invasive detection technologies refer to methods where sensors or probes are directly inserted into the soil for moisture measurement. The traditional gravimetric method is based on the weight difference in soil samples under constant temperature and humidity conditions to calculate SM. However, this method is destructive to the observation site, is significantly dependent on environmental conditions, and is time-consuming [28]. Time Domain Reflectometry (TDR) and Frequency Domain Reflectometry (FDR) determine SM by measuring the propagation period or phase shift in electromagnetic waves, but they require specific calibration with high-cost and complex operation [27,29]. The dielectric constant is also commonly used in SM monitoring, but it is usually affected by soil texture, structure, organic matter content, salinity, and moisture [30]. Capacitance and Impedance Dielectric Reflectometry (CIDR) uses the dielectric constant to analyze the complex impedance of the soil, separating the real and imaginary components of the dielectric constant to distinguish the energy storage and loss of electromagnetic waves, which helps to differentiate salinity, temperature, spatial variability, and moisture between the sensor and soil. Furthermore, it introduces numerical solutions of Maxwell's equations to improve accuracy [31,32]. However, the accuracy of this method decreases with high-moisture soil and needs calibration to address the nonlinearity between voltage and moisture.

2.2. Non-Invasive Detection Technologies

Non-invasive technologies do not directly touch the soil or cause damage. Ground-penetrating radar (GPR) in the L-band can sensitively detect changes in SM. Although these methods offer a high precision and tolerance to surface cover and soil roughness, their accuracy is susceptible to radio-frequency interference (RFI) from the surroundings. So, scholars have proposed a dual-antenna design and a method based on the chirp ratio to measure SM by utilizing phase shifts in LoRa signals, effectively reducing signal interference and improving measurement accuracy [29]. Nuclear Magnetic Resonance (NMR) measures SM by detecting atomic resonance in a magnetic field. This method is highly accurate but requires expensive equipment, is hard to operate, and has high demands for the magnetic field [33]. A Cosmic Ray Neutron Probe (CRNS) infers SM by measuring the number of slow neutrons generated from collisions between fast neutrons and hydrogen atoms in the soil. The number of slow neutrons is proportional to the SM [33]. The novel CRNS-FINAPP detector, based on scintillators, offers a high sensitivity and is suitable for large-scale SM monitoring. However, it faces challenges such as high operation costs, radiation exposure, and a limited observation range [34]. The applicability of in situ observation-based monitoring methods varies significantly across different situations. Table 1 summarizes the characteristics and applicability of current in situ observation methods.

Table 1. Comparison of advantages and limitations of in situ soil moisture monitoring techniques.

Technique	Advantage	Limitation	References
Resistive sensors	Low cost Simple structure Long-term monitoring	Temperature sensitivity Salinity sensitivity Low accuracy Soil type sensitivity	[35]
Capacitive sensors	High accuracy after calibration Low initial cost Adaptive application	Complex electronics High cost Soil type sensitivity Temperature sensitivity Limited long-term monitoring	[35,36]

Table 1. *Cont.*

Technique	Advantage	Limitation	References
Ground-penetrating radar (GPR)	Minimal disturbance Large area coverage High resolution	Topography sensitivity Vegetation sensitivity High reflection sensitivity	[35,37]
Tensiometers	Low cost Long-term monitoring	Soil type sensitivity Time-consuming Expensive maintenance	[35,36]
Lysimeters	Easy installation Adaptive application	Temperature sensitivity Calibration required High maintenance effort	[38,39]
Soil moisture meter	Automatic measurement Low maintenance effort Large area coverage	Complex equipment High cost High maintenance effort	[36,40]
FDR	High accuracy Adaptive application High temporal and spatial resolution	Calibration required High cost High maintenance effort	[9,41]
TDR	Long-term monitoring High temporal and spatial resolution	Complex electronics High cost Soil type sensitivity	[9,40,42]
CRNS	Large area coverage Minimal disturbance	Radiation exposure High cost Soil depth sensitivity	[3,27,43,44]

2.3. Key SM Field Experiments and the Global Role of the ISMN

In recent years, major international SM field experiments have provided essential datasets that support algorithm development, product validation, and improvements in the global applicability of passive and active microwave RS. The CanEx-SM10 field experiment established a high-resolution ground–airborne L-band observation benchmark that enabled the pre-launch validation of SMOS/SMAP products, providing essential datasets for the calibration and parameter optimization of SM retrieval algorithms [45,46]. SMAPVEX12 and SMAPVEX16 further contributed through coordinated airborne L-band radiometry and a temporary SM network, offering robust references for SMAP algorithm calibration and accuracy assessment [47,48]. Similarly, the SMAPEx provided dense multi-season observations that have been critical for evaluating SMAP performance in arid and semi-arid regions [49].

Regional programs have also played an important role. THEXMEXs generated systematic datasets on SM heterogeneity in drylands, supporting microwave model evaluation for complex surfaces [50]. The MicroWEXs, through plot-scale networks and surface flux observations, advanced the understanding of microwave brightness temperature–SM relationships and scale transition modeling [47]. The AMMA project established a multi-scale SM observations system widely used for evaluating satellite product stability and studying land–atmosphere feedback [51,52].

In addition, the International Soil Moisture Network (ISMN) provides standardized, quality-controlled global in situ SM records, serving as a consistent foundation for satellite validation, model calibration, and uncertainty assessment [53,54]. Its continuous expansion greatly enhances the global verifiability and cross-regional applicability of satellite SM products.

The establishment of a comprehensive and well-organized ground-based SM observation network has fundamentally improved the previously fragmented validation practices

of satellite SM products. As demonstrated by the work of Gruber et al., the network enables a complete and standardized validation workflow—from data selection and preprocessing to uncertainty quantification—effectively resolving the long-standing issue of non-comparable evaluation results caused by the heterogeneity of traditional reference datasets [55].

3. Remote Sensing-Based Soil Moisture Inversion Methods

Remote sensing (RS) inversion offers significant advantages for large-scale ground exploration, with the ability to provide coherent information across spatial and temporal scales. Therefore, RS-based observation methods have been widely applied to soil moisture (SM) inversion.

3.1. Optical RS-Based Estimation Methods

Optical RS technology operating in the visible light spectrum (0.3–0.76 μm) provides a preliminary analysis of the physics of the soil surface and vegetation cover by capturing reflections from the surface of vegetation, soil, and others across different wavelengths, which is highly sensitive to water movement and can indirectly offer valuable information for SM inversion. Within the infrared wavelength range (0.76–100 μm), the thermal radiation properties of soil and vegetation serve as key indicators, and variations in SM significantly affect the thermal inertia and thermal–hydrological balance, thereby altering the soil surface temperature distribution. Consequently, these temperature differences can be precisely detected by infrared RS to effectively invert SM dynamics [11]. The fusion of visible and infrared RS technologies provides a more stable observation approach for accurate and efficient SM inversion compared with using a single RS method [56,57].

3.1.1. RS Index Method

The RS index, as a key parameter for surface conditions, is a sensitive indicator of humidity-related information for the land surface and atmosphere. However, the index method is primarily limited by its shallow sensing depth and is susceptible to interference from spatiotemporal relationships, spatial heterogeneity, surface biological properties, and evapotranspiration (ET) [58,59], making it difficult to effectively invert dynamic changes in the vertical soil profile. By using the Soil Water Index (SWI) [60], the spatiotemporal variation characteristics of SM can be incorporated into a two-layer water balance model to consider moisture at different layers, avoiding interference and more fully accounting for the moisture balance and natural water storage changes in soil. Therefore, it improves the accuracy and spatial resolution of SM inversion [58,61]. The water balance relationship under the two-layer model performs well in inversing SM and soil aridity, but it heavily relies on prior data, environmental parameters, and the algorithms employed [62]. Thus, it is not suitable for regions where environmental parameters are hard to obtain or where there is no support from in situ measurements. Moreover, this method may overestimate drought severity in arid areas [63]. The complexity of surface vegetation also influences the inversion results. The Vegetation Temperature Condition Index (VTCI) and SWI focus on surface covering, since vegetation has a clear response to water volume inside roots. Therefore, the relationship between vegetation and land surface temperature (LST) can effectively reveal the SM result [64,65]. However, this method is easily influenced by the vegetation density [66], and spectral reflections of vegetation can be easily interfered with by atmospheric status, the scale and type of observation, and vegetation growth [67,68]. Carlson et al. constructed a feature space for pixels using the vegetation index (VI) and LST by treating the geometric distribution of pixels as the boundary. Known as the triangular method, this approach does not require detailed atmospheric status or

prior soil data and reduces the need for atmospheric calibration by scaling the observation variables [69,70]. However, the dry–wet boundary is highly influenced by atmospheric forcing and unreal dry–wet points, inaccurate dry–wet boundaries, and incorrect ET estimation exist in large-scale space [71]. This method cannot accurately capture deep SM and vegetation water volume. For the trapezoidal method, an improvement over the triangular method, the subjective determination of pixel windows, and the assumption of similar atmospheric conditions for a comparison of each pixel's spatial distribution are required [72]. Moreover, LST is influenced not only by SM but also by environmental atmospheric conditions, making the triangle and trapezoidal methods difficult to apply across different regions and times since they significantly rely on empirical or semi-empirical models [73]. Inge Sandholt and colleagues proposed a simpler Temperature Vegetation Drought Index (TVDI) based on Carlson's research [74]. This method does not require meteorological or ground observation data. Instead, it parametrizes the relationship between the temperature of the surface (Ts) and the Normalized Difference Vegetation Index (NDVI) to perform inversion, providing more detailed vegetation and moisture information [75]. However, it is suitable for low vegetation coverage areas (vegetation coverage < 35%), which should not be too low, as insufficient vegetation coverage can lead to inaccurate identification for drought, and should not be too high, since too much vegetation covering reduces NDVI sensitivity and causes large deviations. This method is also sensitive to the directional anisotropy of LST, which can cause inconsistencies in results at different observation angles [76]. The temporal error in LST and NDVI can affect the extraction of the dry–wet boundary, leading to inversion errors [77]. Additionally, precipitation and ET are closely related to hydrological processes. Incorporating ET into the index calculation can improve the accuracy of SM evaluation [78]. The modified perpendicular drought index (MPDI) reflects SM variations, playing a significant role in assessing the spatiotemporal distribution of drought under global climate change [79], monitoring spatial heterogeneity of drought in agricultural areas, constructing global drought index datasets [80,81], and monitoring global warming and wetting trends [79]. There are numerous methods for inversing SM using RS indices. The examples mentioned above focus on spatial complexity, biological influences, and ET. More methods are detailed in Table 2.

Table 2. Summary of soil moisture inversion methods and functions based on remote sensing indices in published order. Strong correlation: can be directly used for quantitative inversion of soil moisture; weak correlation: indirect inversion of soil moisture through vegetation status.

Correlation	Indices	Categorization	Functions	References
Strong correlation	CWSI	Energy-related Indices	Based on Evapotranspiration (ET): $CWSI = 1 - ET/PET$ Canopy–Air Temperature Difference (ΔT)-Based: $CWSI = \frac{Tc-Ta}{Tdry-Ta}$ Theoretical Model-Based: $\mathrm{CWSI} = \frac{(T_c-T_a)-\left(\Delta\times\frac{R_n}{\rho\ \times\ C_p\ \times\ \left(1+\frac{\gamma}{r_H}\right)}\right)}{\left(T_{dry}-T_a\right)-\left(\Delta\times\frac{R_n}{\rho\ \times\ C_p\ \times\ \left(1+\frac{\gamma}{r_H}\right)}\right)}$	[82–84]
	TSMI	Vegetation Status Indices	$TSMI = c_0 + \sum_{i=1}^{10} ci\ pi$	[85]

Table 2. *Cont.*

Correlation	Indices	Categorization	Functions	References
Strong correlation	WDI	Energy-related Indices	Based on Evapotranspiration (ET): $WDI = 1 - ET/PET$ TVDI-Based Approaches: $WDI = \frac{TVDI - TVDImin}{TVDImax - TVDImin}$	[86]
	SWI	Moisture Indices	$SWI = \frac{SM - SM_{\min}}{SM_{\max} - SM_{\min}}$	[61]
	TVDI	Energy-related Indices	$TVDI = \frac{Ts - Tsmin}{a + b \times NDVI - Tsmin}$	[74]
	SIWSI	Energy-related Indices	$SIWSI = \frac{R_{SWIR} - R_{NIR}}{R_{SWIR} + R_{NIR}}$	[87]
	ESMI	Energy-related Indices	$ESMI = NDVI/\alpha$	[88]
	MPDI	Drought Indices	$MPDI = \frac{PDI - f_v PDI_v}{1 - f_v}$	[89]
Weak correlation	VTCI	Energy-related Indices	$\mathrm{VTCI} = \frac{\mathrm{LST}_{\mathrm{NDVI,max}} - \mathrm{LST}_{\mathrm{NDVI}}}{\mathrm{LST}_{\mathrm{NDVI,max}} - \mathrm{LST}_{\mathrm{NDVI,min}}}$	[65]
	VCI	Vegetation Status Indices	$\mathrm{VCI} = \frac{(NDVI - NDVI_{min})}{(NDVI_{max} - NDVI_{min})} \times 100$	[90,91]

3.1.2. Thermodynamic and Energy Balance Methods

Changes in the thermodynamic state of soil are the key indicators for the movement of moisture. The thermodynamic characteristics of soil, such as thermal capacity and thermal conductivity, are significantly influenced by SM and changes in thermal properties, caused by thermodynamic variations, which directly reflect SM. By building empirical or semi-empirical models to describe a relationship between thermodynamic variables and SM, it is possible to invert the changes in SM under more complex scenarios. The general process for this SM inversion is shown in Figure 4.

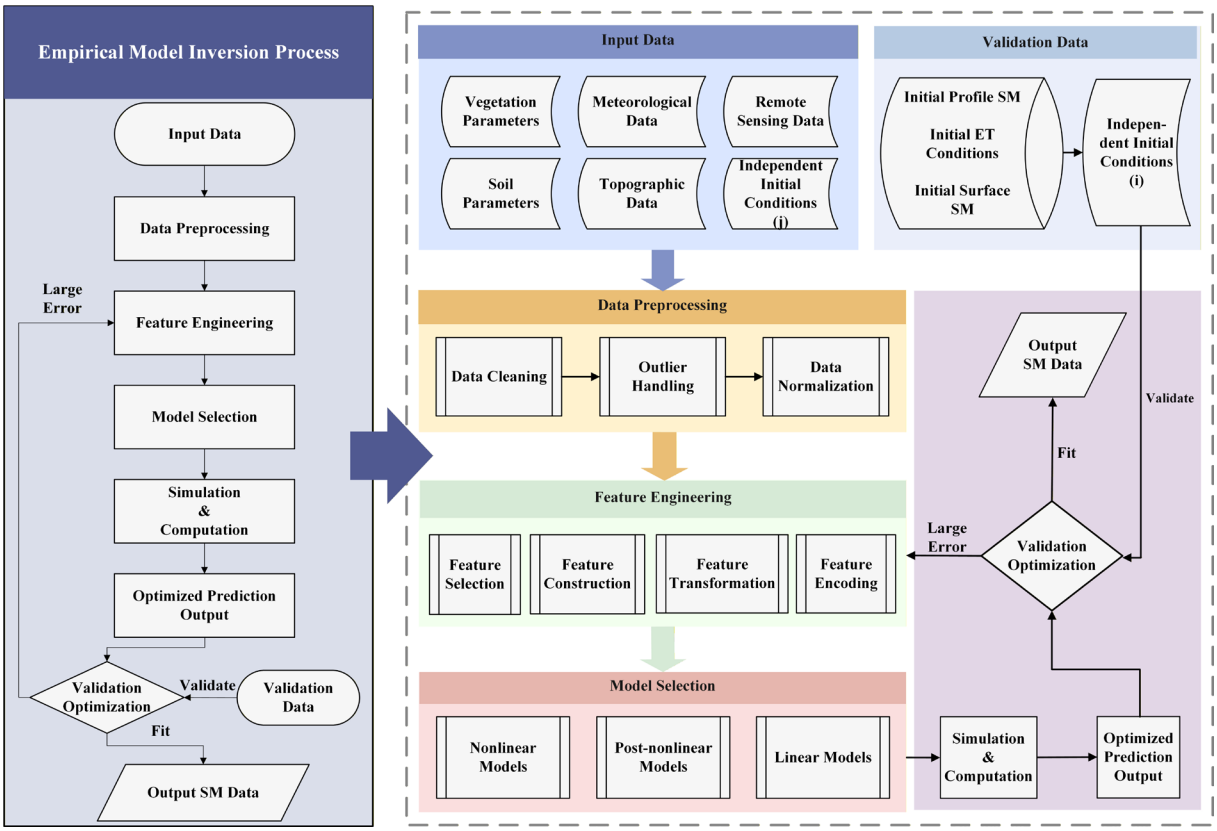


Figure 4. SM inversion process based on empirical and semi-empirical models.

Among thermodynamic approaches, thermal–infrared RS (TIR)-based inversion remains one of the most widely used and physically interpretable methods. By combining LST with VI, texture indices, and thermal infrared vegetation indices, TIR-based approaches capture the sensitivity of surface temperature to SM, particularly in sparsely vegetated regions where the thermal signal is strongly controlled by soil evaporation [92]. Recent work has further shown that red-edge and short-wave infrared bands from Sentinel-2 improve SM retrieval in mixed vegetation–soil pixels, extending their applicability to more heterogeneous conditions [93]. For complex terrain, topographic correction using MODIS LST products has been shown to reduce the retrieval biases caused by temperature discontinuities [70].

A second major category is the thermal inertia (TI) method, which exploits the dampening effect of SM on diurnal temperature variations. The classical TI framework [92] has been simplified through the apparent thermal inertia (ATI) formulation [94], and subsequently improved by incorporating soil porosity and simulating multiple soil textures [95,96]. These advances reduce parameter uncertainty and enhance applicability across varying soil structures and vegetation cover. High-resolution multispectral and thermal infrared data from UAV platforms further refine thermal property estimation and significantly enhance SM inversion accuracy in heterogeneous landscapes [97]. Although TI-based approaches remain computationally intensive, they are among the most thermodynamically consistent methods for retrieving SM at diurnal to seasonal scales.

In addition, surface energy balance-based SM estimation provides a physically grounded and generalizable framework. Rather than relying on full evapotranspiration (ET) modeling, recent SM-oriented applications focus on the relationship between LST, VIs, and the partitioning of available energy, enabling the identification of dry and wet endmembers and deriving SM through normalized evaporative indices [98]. This family of methods builds on the premise that SM strongly regulates the ratio of sensible to latent heat fluxes, and recent studies have demonstrated an improved performance when incorporating high-resolution LST, vapor pressure deficit, and land–surface coupling metrics [99]. These developments significantly enhance the robustness of energy balance-based SM estimation while avoiding the limitations of ET-focused models such as SEBAL or the Penman–Monteith equation, whose detailed parameterization is not primarily designed for SM retrieval.

Collectively, these thermodynamic and energy balance approaches provide an important complementary pathway to microwave-based SM inversion. Their strengths include high responsiveness to surface evaporative conditions, strong physical interpretability, and the ability to leverage optical, thermal, and UAV data sources for improving spatial detail and extending applicability across diverse land surface conditions [100].

3.2. Active and Passive Microwave Radiation and Radiation Transfer Modeling-Based Methods

Changes in SM lead to fluctuations in dielectric constants, causing significant differences in the propagation characteristics of microwave signals in the soil layer (phase and polarization). By investigating the changes in these signals, SM can be inverted. The microwave method relies primarily on the dielectric properties of soil, which are strongly influenced by SM. Microwave inversion can be categorized into passive microwave RS and active microwave RS. Commonly used frequency bands include P-band (0.3–1 GHz), L-band (1–2 GHz), C-band (4–8 GHz), X-band (8–12 GHz), Ku-band (12–18 GHz), and Ka-band (26.5–40 GHz). Different bands have respective advantages towards SM, soil texture (sand or clay), soil salinity, and the ability to penetrate vegetation cover [101]. In practical applications, the X-, Ku-, and Ka-bands are generally unsuitable for SM retrieval. These higher-frequency signals are strongly attenuated by vegetation canopies and have limited

penetration depths compared with the L-band [102]. They are also more sensitive to surface roughness, causing scattering contributions to dominate and thereby suppressing inversion sensitivity [103,104]. Studies further show that X-band SAR performs poorly in densely vegetated areas [105], and earlier analyses indicate that Ku- and Ka-band responses to soil parameters are weak, with variations driven mainly by surface scattering and vegetation rather than SM [106–108].

In contrast, P-, L-, and C-band microwaves provide more favorable characteristics for SM inversion. The P-band penetrates surface roughness and sparse vegetation and is sensitive to deeper soil dielectric variations, with minimal roughness or vegetation interference [109]. The L-band offers the best balance between soil dielectric sensitivity and vegetation penetration, which is why it is adopted by major missions such as SMOS, SMAP, and ALOS-PALSAR [110–112]. The C-band retains useful sensitivity to surface moisture, especially in sparsely vegetated regions, and its high revisit frequency is valuable for trend analysis and data assimilation [112].

The direct connection between microwave signals and SM inversion or the relationship between the radiation signal and the physical processes can be utilized, as illustrated in Figure 5.

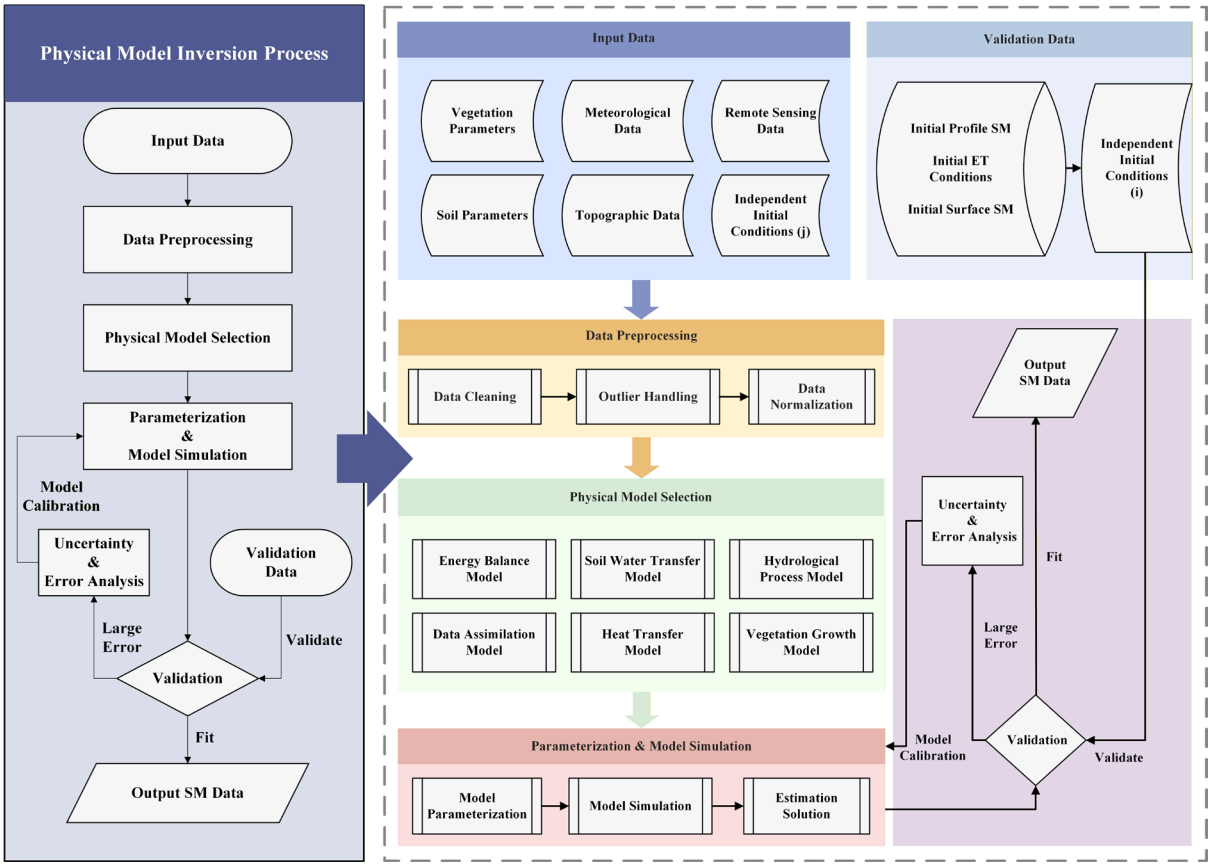


Figure 5. SM inversion process based on physical models.

3.2.1. Active and Passive Microwave Radiation-Based Method

Active microwave radiation imaging has a high spatial resolution and thus is extremely sensitive to surface structure, but its temporal resolution is low. The image processing is complex and is susceptible to the influence of surface roughness. In contrast, passive microwave radiation has a higher temporal resolution, but a lower spatial resolution, since the passive method receives radiation from the surface, which is sensitive to surface moisture and can obtain deeper SM information, but is also sensitive to surface structure.

(a) Active Microwave Radiation RS-Based Methods

Sentinel-1, equipped with C-band active microwave radar, has a wide spatial coverage, is effective in harsh weather conditions, and performs well in areas with vegetation coverage. SAOCOM's L-band, on the other hand, is more sensitive to SM and can effectively avoid the impact of surface structure on the signal. Rana et al. combined the data from both satellites to effectively reduce the impact of soil surface roughness and atmospheric interference on the data [113]. Xing et al. proposed a method to calibrate soil and vegetation parameters using the Water Cloud Model (WCM) and the Ulaby soil model. By integrating Sentinel-1 data with a random forest (RF) algorithm, they achieved high-spatial-resolution inversion of SM and generated a 1 km resolution product (SMS-1), which helps address the accuracy issues caused by a complex vegetation canopy structure [114]. Fan et al. used the τ-ω two-layer radiation transfer model with dual-polarization (VV and VH) to obtain brightness temperature observation data, creating a microwave polarization difference index to calculate SM and vegetation optical depth (VOD). Polarization observation data can capture more detailed surface features and canopy information, reducing the reliance on auxiliary parameters like surface temperature and improving SM inversion accuracy while providing higher spatial resolution products [115]. Combining C-band SAR data with optical data can effectively reduce the impact of vegetation and enhance the temporal and spatial accuracy of inversion data. Wu et al. combined Landsat 8 optical data with SAR data and applied RF models along with optimization algorithms such as Ant Colony Optimization (ACO) and Sparrow Search Algorithm (SSA). By constructing ACO-RF and SSA-RF hybrid models, they addressed the problem of a low spatial resolution and insufficient observation depth in single data source inversions, improving SM inversion accuracy at different depths (0–40 cm) [116]. Optical data can help to optimize empirical or semi-empirical model parameters, thus reducing the impact of vegetation moisture content (VMC) on microwave signal attenuation. Additionally, based on GF-1/3 data, multi-model coupling and background knowledge coupling strategies were used to develop a combined VI model to estimate VWC, enabling high-precision SM inversion in complex surface areas [117]. To better utilize SAR time series data to improve inversion accuracy, a new dual-station radiation transfer modeling framework (RT1) has been applied to process time series data and obtain high-resolution SM information [118]. To describe the nonlinear relationship between radar scattering coefficients and SM, based on AirMOSS-P band radar data, simulated annealing optimization algorithms were proposed to significantly improve inversion accuracy [119].

(b) Passive Microwave RS-Based Inversion Methods

Key parameters affecting the passive microwave RS moisture response include vegetation effective scattering albedo (ω), soil roughness, and VOD, which makes passive microwave susceptible to interference. There are many empirical or semi-empirical parameters when modeling, making the accuracy and applicability of these parameters vary across different regions and scales [120–122]. The uncertainty in model parameters and signal complexity directly affects the accuracy of SM inversion [123,124]. SM is often coupled with vegetation signals. To avoid the influence of multiple parameters, the single-channel algorithm (SCA) is used, which only relies on polarized brightness temperature and VWC to calculate SM, thus reducing the degree of inversion data accuracy degradation caused by multi-parameter coupling. Sharma et al. introduced VWC into the SCA calculation to enhance its application in agricultural irrigation areas, resulting in smaller deviations and stronger correlations compared with the original methods [125]. However, SCAs are based on optical VWC, which is susceptible to weather and cloud interference and is inconsistent with microwave frequencies. To overcome the dependency on vegetation parameters in

SCAs, the Dual-Channel Algorithm (DCA) has been widely applied, which relies only on brightness temperature data, without needing VWC, and uses H/V polarization channels for richer information [126]. Although the DCA does not depend on vegetation parameters, its performance is relatively poor, its algorithm is complex, and its inversion for VWC still requires auxiliary data. In areas with bare soil or sparse vegetation coverage, the difference is insignificant, leading to unstable inversion [127]. Vegetation signal scattering and interannual variations in vegetation optical depth pose a challenge to the accuracy of SM inversion. The fusion of multi-angular observations with active–passive microwave data fusion is a key direction for improving inversion precision [128]. The AMSR2 IB algorithm considers factors such as vegetation coverage, soil texture, and moisture content. Since observation signals are easily influenced by soil roughness, by calibrating ω and soil roughness, it uses the τ-ω radiation transfer model for the inversion of SM and VOD [126,129]. Similarly, using the Deterministic Ensemble Kalman Filter (DEnKF) and other filters for data assimilation [130], along with different land surface data to improve soil parameter estimation, can enhance precipitation estimation and SM inversion accuracy [131].

(c) Global Navigation Satellite System (GNSS) Reflection Methods

In recent years, the use of Global Navigation Satellite System Reflection (GNSS-R) signals for SM inversion has gained significant attention. This includes GNSS-R, GPS Interferometric Reflection Measurement (GNSS-IR), and Multi-GNSS Interferometric Reflection Measurement (Multi-GNSS) technologies [22,132]. The principle of GNSS-R, which is like the SMAP satellite, considers multipath effects, signal-to-noise ratio analysis, geometric relationships, and interference patterns. GNSS signals refract as they pass through soil, and the intensity of the signals is related to the dielectric constant of the soil, achieving SM inversion [133]. GNSS technology does not require extra transmitters and can make full use of existing satellite signals and ground receiving stations, making it low-cost. Its data processing is simple, making it easy to implement large-scale, long-term inversion. By integrating GPS, GLONASS, Galileo, and BDS multi-constellation data, GNSS technology can achieve global coverage, compensate for missing data series, and improve applicability. With advanced algorithms, GNSS technology can process data in real time, offering a high temporal resolution and the ability to capture rapid changes in SM.

3.2.2. Radiation Transfer Modeling-Based Methods

The soil dielectric constant changes with SM, which in turn affects the brightness temperature observed by microwave radiometers. SM can be inverted by establishing models between the brightness temperature and SM, which primarily have three categories: dielectric model methods, soil roughness model methods, and vegetation–surface radiation transfer process simulation methods (RTMs).

(a) Dielectric Model Method

SM directly influences the dielectric constant of the soil. By applying the Fresnel reflection equation, a mathematical relationship can be established between reflectance and the dielectric constant of the surface, which can then be used to invert SM [134]. As early as 2014, several dielectric methods have been proposed to estimate SM for SMAP satellite data, such as the Mironov, Dobson, Wang_Schmugge, and Hallikainen models [135]. In 2015, Mialon et al. compared the response of various dielectric models on a global scale, finding that the Mironov model required fewer input parameters while exhibiting a higher correlation [136]. Meanwhile, in 2021, Suman et al. tested the response of mixed dielectric models in complex terrains, providing valuable insights for selecting the most suitable

model in various terrain and climate conditions [137]. But other factors, such as surface roughness [138], vegetation cover, soil texture [139], soil salinity [140], and temperature, can also impact the accuracy of dielectric constant measurements. While the dielectric constant method provides the foundational physics for RTM inversion, the research focus is shifting towards the roughness of soil and vegetation water content, aiming to achieve a higher precision by mitigating the effects of interference and scale discrepancies.

(b) Soil Roughness Model Method

Soil roughness is a crucial parameter influencing microwave signal interactions, and traditional models often rely on semi-empirical methods by comparing the reflection differences between bare soil and smooth surfaces [141]. However, actual soil surface conditions are more complex, and the presence of numerous nonlinear factors can make it hard for simplified linear models to represent the surface conditions. To overcome this, some researchers has proposed using the τ-ω model along with TB and in situ data to simulate soil roughness as a dynamic parameter h rather than a static constant when inversing SM [142]. Meanwhile, another team suggested combining a multi-scale roughness model to invert soil roughness and achieved a good SM validation result in SMAPVEX12 and SMAPVEX15 [143]. In 2021, Yin et al. used a scattering model and combined it with a dual-channel convolutional neural network (CNN) to build the nonlinearity between SM and roughness, allowing for the more precise inversion of SM variations [144]. A method for implementing the RF model to calibrate global soil roughness for SMOS-IC SM inversion was also published [145]. More recent research has taken a geometric perspective. By using the Integral Equation Model (IEM) with SAR data, multi-scale soil roughness estimates have been obtained, enhancing SM inversion accuracy [146]. With more studies and research into soil roughness, we can be convinced that soil roughness performs as a coupled system with SM, making it difficult to accurately invert each parameter in isolation [147]. Moreover, in densely vegetated areas, the vegetation interference further obscures their individual signatures and becomes the primary source of retrieval error [138].

(c) Vegetation–Surface Radiation Transfer Process Simulation Method

Vegetation–surface RTMs are essential for microwave-based SM retrieval in vegetated landscapes because they explicitly separate soil emission from canopy scattering and attenuation [122]. The τ–ω model remains foundational: SM influences soil emissivity via dielectric changes, while vegetation optical depth (τ) and single-scattering albedo (ω) control the vegetation contribution. Recent parameter refinements, accounting for canopy structure and VOD-SM coupling, improve robustness under moderate to dense vegetation [148].

Advanced schemes such as joint SM-VOD-ω retrievals, exemplified by the spatially constrained multi-channel algorithm (S-CMCA), simultaneously estimate these three parameters from L-band observations. This reduces trade-offs and stabilizes SM estimates in heterogeneous cover [104]).

The L-MEB model and simplified variants (e.g., modified τ-ω, H-Q-N) efficiently simulate vegetation–soil interactions with a lower computational cost, improving retrieval in structurally complex canopies [126,149]. Two-stream (2S) models offer more realistic canopy representations by modeling upward and downward radiation, which enhances SM retrieval in tall or multi-layer vegetation compared with τ-ω alone [150].

Frequency-dependent inversion has also advanced: P-band τ–ω modeling improves penetration through dense biomass, reducing bias in forested areas relative to L-band [151]. Finally, 3D and hybrid RTMs, including discrete or stochastic canopy architectures, address the limitations of 1D/2D models by better capturing canopy heterogeneity and structural scattering, which significantly enhances SM estimation in forests [152,153].

In summary, these radiative transfer approaches, ranging from classic τ-ω to multi-parameter inversion and 3D modeling, directly contribute to more accurate, physically grounded SM retrieval across different vegetation types.

4. Soil Moisture Products: Main Datasets

Over the years, researchers have accumulated a vast number of soil moisture (SM) datasets by employing different inversion methods across various geographical regions, soil types, and vegetation covers.

In this study, publicly available SM datasets are classified into four primary categories based on their sensor type and inversion method: passive microwave-based, active microwave-based, multi-sensor merged, and reanalysis data-based products. From a physical perspective, this categorization reflects the fundamental differences in sensor characteristics, received signals, and data processing principles.

Passive microwave-based datasets typically rely on brightness temperature (Tb) measured by radiometers or estimating soil dielectric properties via radiative transfer models (RTMs) to invert SM. These products provide long-term time series, global coverage, and a stable large-scale performance, but they generally feature a low spatial resolution and are sensitive to vegetation cover and soil surface roughness.

Active microwave-based datasets are primarily produced using radar observations (SAR or scatter meters) that actively transmit microwave pulses and record the backscattered signals and invert SM through backscattering models. These products offer a higher spatial resolution, ranging from the meter to kilometer scale. Yet they remain vulnerable to the effects of vegetation and surface roughness.

From the perspective of data processing strategies, SM datasets can also be categorized as multi-sensor merged products or reanalysis data-based products. Reanalysis data-based SM is generally not inverted directly from satellite observations. Instead, it is generated by land surface models (LSMs) coupled with data assimilation techniques. These datasets exhibit strong spatial–temporal continuity, but their accuracy may be influenced by model inputs and parameterization processes.

In contrast, multi-sensor merged products typically estimate SM indirectly using variables such as land surface temperature (LST), vegetation indices (NDVI), and evapotranspiration models. Such products usually have higher spatial resolutions; however, because they predominantly rely on optical RS, they are generally limited to shallow surface SM, are susceptible to cloud contamination, and their accuracy can be affected by the indirect nature of the modeling workflows.

These datasets provide critical data for in-depth analysis and research. To comprehensively explain these datasets and provide precise data sources for subsequent research, the following table (Table 3) summarizes existing publicly available SM data products and describes the characteristics of each dataset.

Table 3. Summary of publicly available soil moisture products, with all links verified as of 4 December 2025; the information in the table is primarily based on Fan et al. [115], with updates, improvements, and additional data contributed by us.

Products	Institutions or Data Centers	Category	Spatial Coverage	Sensors or Models	Spatial Resolution	Temporal Coverage	Temporal Resolution	Sensing Depth	Advantages	Limitations	Data Links	References
AMSR-2 L3	JAXA	Passive microwave-based	Global	AMSR2	50 km	2012–now	1–2 days	0–5 cm	Multiple signals Supports ecological studies	Vegetation and surface sensitivity	https://www.eorc.jaxa.jp/AMSR/index_en.html (accessed on 21 October 2025)	[154]
AMSR-E L2/L3	JAXA/ NASDA	Passive microwave-based	Global	AMSR-E	50 km	2002–2011	1–3 days	0–5 cm	Moderate spatial coverage Frequent observations	Discontinued in 2011 Vegetation and surface sensitivity	https://www.eorc.jaxa.jp/AMSR/index_en.html (accessed on 21 October 2025)	[155]
LPRM AMSR-E	VUA/NASA	Passive microwave-based	Global	AMSR-E	25 km	2002–2011	1–3 days	0.5–1.5 cm	Detailed land surface information Well calibrated and validated Good consistency within in situ data	Discontinued in 2011 Vegetation and surface sensitivity	https://www.geo.vu.nl/~jeur/lprm/ (accessed on 21 October 2025)	[156]
AMSR Unified L2B	NSIDC	Passive microwave-based	Global	AMSR-E/AMSR2	25 km	2012–now	1–2 days	0.5–1.5 cm	Supports trend analysis and climate study	Vegetation and surface sensitivity Susceptible to RFI Incomplete datasets Requires careful calibration/validation	https://nsidc.org/data/au_land/versions/1 (accessed on 21 October 2025)	[157]
MCCA AMSR	AIRCAS/ TPDC	Passive microwave-based	Global	AMSR-E/AMSR2	0.25°	2001–2022	1–2 days	surface soil	Supports trend analysis	Requires extensive processing Vegetation and surface sensitivity	https://data.tpdc.ac.cn/en/data/034b78c9-80d1-47f1-9e19-eeaf2a309010/ (accessed on 21 October 2025)	[158,159]
NNsm	THU/ AIRCAS	Passive microwave-based	Global	AMSR-E/AMSR2	36 km	2002–now	1–2 days	surface soil	Supports trend analysis	Limited spatial resolution Algorithm limitations reduce accuracy in certain regions	https://data.tpdc.ac.cn/home (accessed on 21 October 2025)	[158,160]

Table 3. *Cont.*

Products	Institutions or Data Centers	Category	Spatial Coverage	Sensors or Models	Spatial Resolution	Temporal Coverage	Temporal Resolution	Sensing Depth	Advantages	Limitations	Data Links	References
DS-AMSR	TPDC	Reanalysis data-based	China	AMSR-E/AMSR-2/MODIS	1 km	2003–2023	1 day	0–10 cm	Suitable for regional analysis Cloud gap filling (improved completeness)	Limited to China Vegetation and surface sensitivity Requires careful calibration/validation	https://data.tpdc.ac.cn/home (accessed on 21 October 2025)	[161]
AQ3_ANSM	NSIDC	Passive microwave-based	Global	Aquarius	1°	2011–2015	1 day	surface soil	Reliable SM measurements Suitable for large-scale climate studies	Limited to fine-scale research Short temporal span	https://nsidc.org/data/aquarius/data (accessed on 21 October 2025)	[162].
ASCAT NRT	EUMETSAT H-SAF	Active microwave-based	Global	ASCAT	10/12.5/25/50 km	2007–now	1–2 days	1–2 cm	Flexible spatial resolution options	Vegetation and surface sensitivity Requires calibration	https://hsaf.meteoam.it/ (accessed on 21 October 2025)	[163,164]
SMRFR	ISMN/ERA5-Land	Reanalysis data-based	Global	ASCAT/SMOS	9 km	2000–2023	1 day	0–100 cm	Suitable for long-term studies	Insensitivity to extreme events Larger errors in complex terrain	https://figshare.com/articles/dataset/_b_SMRFR_Global_multilayer_soil_moisture_dataset_with_spatiotemporal_dynamic_insights_using_machine_learning_b_/27601035?file=50173440 (accessed on 21 October 2025)	[165]
ASCAT NRT DIS	EUMETSAT H-SAF	Active microwave-based	Europe	ASCAT	1 km	2007–now	1–2 days	0–7 cm	Applicable globally	Limited to Europe Atmosphere and surface sensitivity	https://hsaf.meteoam.it/ (accessed on 21 October 2025)	[163,164]

Table 3. *Cont.*

Products	Institutions or Data Centers	Category	Spatial Coverage	Sensors or Models	Spatial Resolution	Temporal Coverage	Temporal Resolution	Sensing Depth	Advantages	Limitations	Data Links	References
ESA CCI	ESA	Multi-sensor merged	Global	ASCAT/SMMR/ SSM-I/TMI/ AMSR-E/ WindSat/FY/ AMSR2/SMOS/ GPM/SMAP	0.25°	1978–now	1 day	0–5 cm	Suitable for climate studies Comprehensive data Improved performance with multi-sensor integration	Non-uniform data quality Requires extra processing	https://archive.ceda.ac.uk/ (accessed on 21 October 2025)	[166]
CCI 9 km	PANGAEA	Multi-sensor merged	Global	CCI/SMAP	9 km	1978–2020	1 day	0–5 cm	Suitable for detailed analysis Comprehensive data Accurate simulation	Local details missed Requires extensive processing	https://doi.pangaea.de/10.1594/PANGAEA.940409 (accessed on 21 October 2025)	[167,168]
GLASS	WHU/UMD	Reanalysis data-based	Global	ERA5-Land/ GLASS/ISMN	1 km	2000–2020	1 day	0–5 cm	Improved performance with multi-sensor integration	Requires careful calibration/validation	http://glass.umd.edu/soil_moisture/ (accessed on 21 October 2025)	[169]
ERS-2	TU/ESA	Active microwave-based	Global	ERS AMI WS	25/50 km	1991–2011	1–2 days	0.5–2 cm	Compatible with other soil moisture datasets	Discontinued in 2011 Requires extensive processing Requires careful calibration/validation	https://earth.esa.int/eogateway/activities/sciroccо (accessed on 21 October 2025)	[61]
DS-CCI	TPDC/ AIRCAS	Reanalysis data-based	Global	ESA-CCI/ERA5/ MODIS/ISMN	1 km	2000–2020	1 day	0–3 cm	Comprehensive soil moisture inversion	Inconsistent inversions	https://data.tpdc.ac.cn/en/data/30131436-88d1-4be3-8e3d-14905a29d6d6/ (accessed on 21 October 2025)	[170]
NNsm FY	AIRCAS/ TPDC	Passive microwave-based	Global	FY-3B	25 km	2010–now	1–2 days	1–5 cm	Suitable for trend and climate studies	Vegetation and surface sensitivity	https://data.tpdc.ac.cn/home (accessed on 21 October 2025)	[81]

Table 3. *Cont.*

Products	Institutions or Data Centers	Category	Spatial Coverage	Sensors or Models	Spatial Resolution	Temporal Coverage	Temporal Resolution	Sensing Depth	Advantages	Limitations	Data Links	References
FY-3C/D	NSMC	Passive microwave-based	Global	FY-3C/D	25 km	2014–now	1–2 days	0–1 cm	Suitable for agriculture, irrigation, and weather forecasting	Vegetation and surface sensitivity	https://satellite.nsmc.org.cn/DataPortal/cn/home/index.html (accessed on 21 October 2025)	[171]
MERRA-2	NASA	Reanalysis data-based	Global	GEOS ADAS Model	0.5° × 0.625°	1980–now	1 day	0–100 cm	Accurate simulation	Local details missed	https://climatedataguide.ucar.edu/climate-data/nasas-merra2-reanalysis (accessed on 21 October 2025)	[172–174]
GLDAS-2	NASA	Reanalysis data-based	Global	GLDAS Noah Land Surface Model	0.25°	1948–2014	3 h	0–200 cm	Accurate simulation Near-real-time data Deep SM inversion	Limited soil factor representation Local details missed	https://search.earthdata.nasa.gov/search?q=GLDAS_NOAH025_3H_2.0 (accessed on 21 October 2025)	[175,176]
GLEAM	GHENT/BELSPO/ESA	Reanalysis data-based	Global	GLEAM-Hydro Model	0.1°	1980–2023	1 day	0–250 cm	Accurate simulation Flexible data selection	Computationally intensive Local details missed	https://www.gleam.eu/ (accessed on 21 October 2025)	[177,178]
SMOPS	NOAA	Multi-sensor merged	Global	GPM/SMAP/GCOM-W1/MetOp-B	0.25°	2012–now	6 h	0–10 cm	Near-real-time data	Dependent on other models/data for assimilation and fusion Restricted to specific regions	https://www.ospo.noaa.gov/products/land/smops/ (accessed on 21 October 2025)	[179,180]
SMAP-HB	PU	Reanalysis data-based	USA	HydroBlocks Model/SMAP	30 m	2015–2019	6 h	0–5 cm	Accurate simulation Supports fine-scale analysis	Computationally intensive	https://waterai.earth/smaphb/ (accessed on 21 October 2025)	[181]

Table 3. *Cont.*

Products	Institutions or Data Centers	Category	Spatial Coverage	Sensors or Models	Spatial Resolution	Temporal Coverage	Temporal Resolution	Sensing Depth	Advantages	Limitations	Data Links	References
ERA5-Land	ESA	Reanalysis data-based	Global	IFS Model	0.1°	1950–now	1 h	0–7 cm, 0–289 cm	Accurate simulation Supports fine scale Better soil type and saturation modeling	Weak performance in high latitudes Computationally intensive Local details missed	https://cds.climate.copernicus.eu/datasets/reanalysis-era5-land?tab=overview https://cds.climate.copernicus.eu/datasets/reanalysis-era5-land?tab=overview (accessed on 21 October 2025)	[181,182]
CLMS SSM	Copernicus	Active microwave-based	Europe	Sentinel-1	1 km	2014–now	1–3 days	Surface soil	Supports fine-scale analysis	Limited to Europe Vegetation and surface sensitivity	https://land.copernicus.eu/en/products/soil-moisture (accessed on 21 October 2025) https://documentation.dataspace.copernicus.eu/Data/CopernicusServices/CLMS.html (accessed on 21 October 2025)	[112]
DS-SMAP	UVA/NSIDC	Passive microwave-based	Global	SMAP	1 km	2015–now	1–2 days	0–5 cm	Supports fine-scale analysis	Weak performance in high latitudes and cold seasons	https://nsidc.org/data/nsidc-0779/versions/1 (accessed on 21 October 2025)	[183]

Table 3. *Cont.*

Products	Institutions or Data Centers	Category	Spatial Coverage	Sensors or Models	Spatial Resolution	Temporal Coverage	Temporal Resolution	Sensing Depth	Advantages	Limitations	Data Links	References
MCCA SMAP	AIRCAS/ TPDC	Passive microwave-based	Global	SMAP	36 km	2015–now	1–2 days	0–5 cm	Reduced dependence on auxiliary data	Limited accuracy in complex vegetation High processing complexity Require auxiliary data in some cases	https://data.tpdc.ac.cn/en/data/591bb9c8-ed6f-4e86-8372-de1c39ba0283/ (accessed on 21 October 2025)	[184]
SMAP_A L2/L3	NSIDC	Active microwave-based	Global	SMAP	3 km	2015	1–3 days	0–5 cm	Accurate simulation	Limited to 2015 data Vegetation and surface sensitivity	https://nsidc.org/data/smap/data (accessed on 21 October 2025)	[185,186]
SMAP_P L2/L3	NSIDC	Passive microwave-based	Global	SMAP	9/36 km	2015–now	1–2 days	0–5 cm	Flexible data selection	Atmosphere and surface sensitivity Incomplete data	https://nsidc.org/data/smap/data (accessed on 21 October 2025)	[111,187]
SMAP-IB	INRAE BORDEAUX	Passive microwave-based	Global	SMAP	36 km	2015–now	1–2 days	0–5 cm	Accurate simulation	Seasonal changes and vegetation conditions sensitivity Weak performance in high latitudes	https://ib.remote-sensing.inrae.fr/ (accessed on 21 October 2025)	[124]
SMAP AP	NSIDC	Multi-sensor merged	Global	SMAP Radiometer/ SAR	3/9 km	2015	1–3 days	0–5 cm	Supports various applications Accurate simulation	Vegetation and surface sensitivity Limited to 2015 data	https://nsidc.org/data/spl3smap/versions/3 (accessed on 21 October 2025)	[188]
RSSSM	PANGAEA	Multi-sensor merged	Global	SMAP/ASCAT/ AMSR2/AMSR-E/ SMOS/TMI/FY/ Wind Sat	0.1°	2003–2020	10 days	0–5 cm	Performs well in dry/cold regions	Vegetation and surface sensitivity	https://doi.pangaea.de/10.1594/PANGAEA.940004 (accessed on 21 October 2025)	[189]
SPL2SMAP_S	NSIDC	Multi-sensor merged	Global	SMAP/ Sentinel-1	1/3 km	2015–now	3–12 days	0–5 cm	Supports fine-scale analysis Supports various applications	Low temporal resolution	https://nsidc.org/data/spl3smap/versions/3 (accessed on 21 October 2025)	[190]

Table 3. *Cont.*

Products	Institutions or Data Centers	Category	Spatial Coverage	Sensors or Models	Spatial Resolution	Temporal Coverage	Temporal Resolution	Sensing Depth	Advantages	Limitations	Data Links	References
LPRM SSM/I	VUA/NASA	Passive microwave-based	Global	SMM/I	50 km	1987–2007	2–3 days	0.5–1.5 cm	Suitable for long-term studies	Vegetation and surface sensitivity	https://www.geo.vu.nl/~jeur/lprm/ (accessed on 21 October 2025)	[156]
LPRM SMMR	VUA/NASA	Passive microwave-based	Global	SMMR	0.25°	1978–1987	2–3 days	0.5–1.5 cm	Applicable globally	Requires extensive processing Incomplete data	https://www.geo.vu.nl/~jeur/lprm/ (accessed on 21 October 2025)	[156]
BEC SMOS L3	EBC	Passive microwave-based	Global	SMOS	25 km	2010–now	1 days	0–5 cm	Good data quality and completeness	Sensitive to brightness temperature (TB) data and surface conditions	https://bec.icm.csic.es/data/available-products/ (accessed on 21 October 2025)	[191–193]
BEC SMOS L4	EBC	Passive microwave-based	Global	SMOS	1 km	2010–2022	1 day	0–5 cm	Good data quality and completeness Applicable globally	Sensitive to brightness temperature (TB) data and surface conditions	https://bec.icm.csic.es/data/available-products/ (accessed on 21 October 2025)	[194]
SMOS IC	INRAE BORDEAUX	Passive microwave-based	Global	SMOS	25 km	2010–now	1–2 days	0–5 cm	Applicable globally	Vegetation and surface sensitivity Susceptible to RFI	https://ib.remote-sensing.inrae.fr/ (accessed on 21 October 2025)	[129]
SMOS L2/L3	ESA	Passive microwave-based	Global	SMOS	15/25 km	2010–now	1–2 days	0–5 cm	Applicable globally Supports fine-scale analysis	Vegetation and surface sensitivity Requires extensive processing Susceptible to RFI	https://smos-diss.eo.esa.int/oads/access/ (accessed on 21 October 2025)	[195]
LPRM TRMM	VUA/NASA	Passive microwave-based	Global	TMI	25 km	1997–2015	2–3 days	0–1.5 cm	Good data quality and completeness	Susceptible to RFI	https://www.geo.vu.nl/~jeur/lprm/ (accessed on 21 October 2025)	[156]

5. Analysis and Discussion

Despite remarkable progress in soil moisture (SM) monitoring over the past decades, existing methods still suffer from significant limitations in their practical applications. In situ observations are constrained by spatial scale, deployment conditions, and maintenance costs. Optical remote sensing (RS) approaches are highly sensitive to atmospheric, vegetation, and other environmental factors. Active and passive microwave techniques are strongly affected by surface cover, topography, and spatial heterogeneity, while model-based methods are often limited by parameter uncertainties and oversimplified assumptions. These shortcomings highlight the pressing need for further advancements in SM monitoring, moving beyond single-method frameworks towards integrated systems that combine multi-source data, advanced physical models, and machine learning. Furthermore, the development of standardized validation protocols and cross-regional benchmarks will be essential to ensure the robustness and global applicability of future SM products.

5.1. Overview of Soil Moisture Monitoring Methods

In this section, we summarize and discuss the limitations of several SM monitoring approaches mentioned above, including in situ observation methods, optical RS-based inversion, thermodynamic and energy balance-based approaches, and passive/active microwave remote sensing combined with radiation transfer models.

5.1.1. In Situ Soil Moisture Measurements

In situ observation techniques provide real-time, high-accuracy SM measurements that are essential for applications in agriculture, water resources management, and related fields, thereby supporting timely production and engineering decision-making [196]. However, in practical scenarios, these methods are typically restricted to small-scale and high-sensitivity studies and are unable to provide large-scale or multi-perspective observations. Their broader deployment is further limited by power supply constraints, network and communication requirements [197], operational complexity, environmental disturbances, and the need for long-term maintenance [198]. These limitations often lead to increased costs [199], potential ecological disturbance, and even health risks to operators, particularly in systems involving cosmic ray neutron sensing [200,201]. In addition, the performance is strongly influenced by site-specific soil properties such as salinity, which may introduce measurement uncertainties or degrade sensor stability [202]. Consequently, the spatial applicability of in situ techniques remains limited to a certain extent. Nevertheless, these methods continue to serve as indispensable tools for obtaining high-precision SM observations and remain fundamental for small-scale process studies as well as for the calibration and validation of remotely sensed SM products.

5.1.2. Optical RS and Index-Based Methods

Index-based SM inversion is strongly affected by vegetation cover, atmospheric conditions, terrain and surface roughness, and the physical dependencies embedded in each index. These factors introduce substantial variability in retrieval accuracy. This section provides a simplified yet rigorous explanation of these influences.

(a) Vegetation Cover-Driven Variations in Index Sensitivity

In sparsely vegetated or bare soil areas (NDVI < 0.3), brightness temperature and related microwave indices such as SWI and MPDI maintain a strong sensitivity to SM. Low-frequency microwave observations couple effectively with soil dielectric properties under minimal canopy conditions [203], enabling the direct inversion of near-surface moisture. Temperature-based indices such as TVDI, although constrained by difficulty in defining

the dry–wet edge, often show stable LST–VI relationships [204]. Incorporating NDVI improves the statistical connection with shallow-layer SM, as evidenced in multiple field evaluations [205].

In moderately vegetated regions ($0.3 \leq \text{NDVI} \leq 0.6$), canopy energy dissipation alters the thermal signal, reducing the application of TVDI, CWSI, WDI, and TSMI. The mixed response from transpiration and soil evaporation the requires joint consideration of vegetation status and water availability. For microwave indices such as SWI and MPDI, inversion sensitivity declines [206], necessitating corrections using LAI or VWC or the use of coupled soil–vegetation modeling approaches [207].

In dense vegetation (NDVI > 0.6), both microwave and thermal infrared signals are dominated by canopy water fluxes. Indices such as TVDI and TSMI thus reflect hydrological water stress rather than SM. Accurate inversion requires canopy scattering or radiative transfer models [208] or integration with root water content and reanalysis with ground observations [21]. Vegetation structural differences further introduce systematic inversion biases [209].

(b) Atmospheric, Topographic, and Surface Roughness Effects

Thermal infrared indices (TVDI, TSMI, VTCI, CWSI) are sensitive to atmospheric conditions because accurate LST inversion depends on atmospheric correction. Clouds, aerosols, and water vapor affect radiative transfer, generating LST errors or observation gaps, and weakening VI–LST relationships [210]. In practice, methods such as cloud masking, temporal compositing, and constructing dry–wet boundaries from clear-sky samples are typically employed for mitigation. Topographic features (e.g., slope, and shadow) introduce distortions in illumination and BRDF effects, affecting both the absolute values and the structure relationship between vegetation indices and LST, thereby necessitating topographic correction or terrain-stratified modeling. CWSI depends on canopy–air temperature differences and meteorological variables, particularly VPD; its accuracy relies heavily on the correct construction of the non-water stress baseline [211]. Biases in wind speed, VPD, or reference temperature can significantly distort the correspondence between CWSI and SM.

In contrast, microwave indices (SWI, MPDI) are less influenced by atmospheric interference but exhibit brightness temperature anomalies shortly after rainfall [212], requiring rainfall filtering or temporal smoothing. Additionally, microwave backscatter and brightness temperature exhibit high sensitivities to incidence angle, needing rigorous geometric correction, particularly over undulating terrain [213]. Surface roughness further alters microwave scattering and polarization behavior [214], which affect the response of the soil dielectric constant changes, requiring parameterization or multi-polarization and time series strategies to reduce its impact [215].

5.1.3. Thermodynamics and Energy Balance Methods

Methods based on thermodynamics and surface energy balance offer notable advantages for inverting land surface temperature and, subsequently, SM. However, they also present several limitations. These approaches are highly sensitive to meteorological conditions, land surface temperature, vegetation cover, and aerodynamic resistance [216], which may lead to data loss or reduced accuracy [217]. The surface energy balance equation involves multiple physical process variables, and in practice, substantial uncertainties arise in the estimation of net radiation, soil heat flux, sensible heat flux, and latent heat flux [218]. Calculations of sensible and latent heat fluxes often rely on empirical parameterizations, which hinder accurate flux partitioning and frequently result in incomplete energy balance closure [219], thereby reducing inversion accuracy. In complex terrains such as mountainous regions, spatial heterogeneity in soils, topography, and vegetation

structure further complicates land surface temperature inversion and increases the difficulty of achieving energy balance at the pixel scale [220], limiting the applicability of these methods across different study areas. Moreover, in detecting dynamic processes such as precipitation events, these approaches often exhibit time lags or biases, making it difficult to capture rapid changes in SM [221]. Such limitations are particularly prominent in seasonally frozen regions, where errors in regional SM inversion may become more significant [222,223].

5.1.4. Microwave RS Methods and Radiation Transfer Method

Microwave RS-based SM inversion is inherently dependent on the parameterization of electromagnetic scattering and radiative transfer processes and therefore is highly sensitive to perturbations from signal contamination, vegetation canopy conditions, surface roughness, terrain heterogeneity, and sensor frequency. First, radio-frequency interference (RFI) can introduce systematic biases and increase uncertainties in passive L-band observations, often resulting in data distortion or increased uncertainty, particularly in regions with strong RFI sources [224]. Second, vegetation coverage, canopy structure, and vegetation water content alter the observable vegetation optical depth (VOD) and single-scattering characteristic, substantially attenuating the microwave signal from soil. Standard τ–ω and semi-empirical scattering models rely heavily on prior assumptions related to vegetation type and growth stage, which constrains cross-regional model applicability and leads to inaccuracies in complex vegetated areas [225]. Third, surface roughness and soil texture impose nonlinear impacts on radar scattering. Commonly used semi-empirical models (e.g., Dubois, Oh, IEM) often fail to represent realistic heterogeneous field conditions [226], and roughness parameters are difficult to estimate accurately at large scales, thereby amplifying inversion uncertainties. Fourth, the vertical sensing depth of microwave signals varies with frequency, because shorter wavelengths respond mainly to the near-surface layer, whereas longer wavelengths penetrate deeper, resulting in depth mixing effects influenced by the vertical SM gradient, soil texture, and vegetation cover. Consequently, SM retrieved from a single band or polarization represents an average moisture which may not correspond to the desired soil layer [227]. Fifth, cross-sensor fusion and data assimilation remain challenging due to inconsistencies in observation frequency, polarization, orbital phases, and spatial resolution, which collectively hinder the continuity between temporal sequences and spatial data [228]. Although empirical or semi-empirical priors may improve local retrieval performance, they also introduce additional parameter uncertainties and facilitate bias propagation.

In theory, high-dimensional numerical models from radiative transfer models (RTMs) provide a more comprehensive description of the transmission, scattering, and absorption processes within the soil–vegetation canopy–atmosphere system, thereby offering superior physical interpretability under complex surface conditions. However, these models often suffer from parameterization complexity, sensitivity to canopy multi-scattering and structural heterogeneity, and substantial demands for training data and computational resources [229]. These limitations restrict their operational utility, particularly in regions with a high canopy optical depth or dense vegetation. Overall, although microwave- and RTM-based methods offer a theoretically robust foundation for SM inversion, practical applications require the integration of multi-frequency and multi-polarization observations, robust in situ measurements, and the explicit quantification of parameter uncertainty, such as through sensitivity analysis, error propagation analysis, and other diagnostic tools, to enhance model stability, transferability, and reliability across diverse land surface conditions.

5.2. Analysis of Soil Moisture Data Products

Publicly available SM datasets provide an indispensable foundation for hydrological, agricultural, and climate research by offering long-term and large-scale observations. However, different types of datasets exhibit fundamental differences in spatial scale, temporal coverage, physical interpretability, and uncertainty sources. A systematic evaluation of these differences is essential for clarifying application boundaries and supporting subsequent data assimilation, downscaling, and multi-source fusion strategies.

5.2.1. Optical and Microwave Remote Sensing Datasets

Satellite-based SM products (e.g., SMOS, SMAP, ASCAT, AMSR2, and ESA-CCI) deliver surface SM (approximately 0–10 cm) at global scales with strong temporal continuity, making them valuable for climate analysis and drought monitoring. However, several inherent limitations remain. First, their native spatial resolution is typically low (e.g., 25–50 km), which constrains their applicability in agricultural or watershed-scale studies. Although downscaling approaches can improve spatial detail, their generalization ability strongly depends on the representativeness of the training environment. Second, microwave signals primarily respond to surface moisture, and their penetration depth varies across frequencies, making the retrieved average moisture an imperfect proxy for root water or depth moisture. Deeper-layer inversion therefore requires in situ measurements or physically based models. Third, retrieval accuracy is strongly affected by environmental factors such as vegetation cover [230], surface roughness, freeze–thaw cycles, snow cover, radio-frequency interference (RFI), and soil salinity. These influences vary dynamically in space and time [231], leading to substantial uncertainties when transferring algorithms across regions. To mitigate these issues, satellite–in situ joint validation, triple collocation analysis, and field-based error modeling are commonly employed to assess and correct remote sensing products [232].

5.2.2. Model Simulation and Data Fusion Products

SM datasets derived from land surface models (e.g., Noah, CLM), hybrid modeling frameworks, and multi-source fusion systems (e.g., GLDAS and regional fusion products) offer continuous spatiotemporal coverage and multi-layer SM information, addressing the observational gaps inherent to satellite and ground networks. Their performance, however, is highly sensitive to the quality of data (PET, ET, and soil parameters). Errors in inputs or inaccurate parameters (e.g., soil texture, rooting structure) can propagate through the modeling or assimilation chain. Furthermore, fusion algorithms, from simple weighted averaging to advanced machine learning architectures, can enhance spatial resolution but also introduce new uncertainties related to training bias, the dependence on prior assumptions, and potential overfitting [233]. Purely data-driven fusion products often lack physical constraints and may perform poorly during extreme hydrological events such as droughts, floods, or freeze–thaw transitions [234]. Recently, physics-guided machine learning approaches have emerged as a promising direction, integrating physical laws with data-driven flexibility. To ensure reliability, sensitivity analyses, triple collocation analyses, and calibrations with representative in situ observations are recommended.

5.2.3. Reanalysis Datasets

Reanalysis datasets (e.g., ERA5-Land, MERRA-2, GLDAS) integrate physical models with observational data assimilation to produce long-term, multi-layer SM inversion suitable for climate and hydrological trend analyses. Their errors primarily originate from model assumptions and the inaccuracy of data. Their performance can degrade substantially in regions with complex terrain (e.g., mountainous areas) or extreme climate regimes

(e.g., freeze–thaw and seasonal snow processes) [235]. Recent studies further indicate that reanalysis products exhibit large discrepancies in spatial–temporal correlation and bias patterns, with some datasets tending to overestimate SM in arid areas and underestimate it in humid regions [236]. Consequently, the broad use of reanalysis SM still requires bias correction and continuous evaluation by ground-based observations.

5.3. Research Trends and Future Outlook

The future of SM monitoring will increasingly depend on the integration of multi-disciplinary technologies, particularly artificial intelligence, big data analytics, advanced RS systems, and next-generation ground observation networks. With the upcoming NISAR and ROSE-L missions providing high-quality L-/S-band and multi-polarization SAR observations [237–241], long-standing limitations related to vegetation penetration, multi-scale surface roughness representation, and model structural uncertainty are expected to be substantially mitigated. These datasets will support physics-informed machine learning and deep learning frameworks, enhancing the accuracy and robustness of SM inversion under diverse surface conditions. Future developments are expected to focus on four main directions.

5.3.1. Multi-Source Data Fusion—Enhancing Consistency and Spatiotemporal Coverage

A promising trend is the fusion of L-band SAR, GNSS-R, optical/thermal infrared, reanalysis, and in situ measurements to jointly improve both the accuracy and applicability of SM products [242]. For instance, Zhang et al. in 2023 developed an LSTM-based model integrating GNSS-R data with radiometer observations, yielding a standard deviation of 0.013 m^3/m^3 in SM retrieval [243]. However, fusion is challenged by inconsistent calibration, mismatched spatial and temporal resolutions, and different sensing mechanisms. Researchers often mitigate these issues via data assimilation, cross-scale normalization, and uncertainty-weighted fusion. Yet, uncertainty quantification across different sources is not yet standardized, and high-accuracy, globally distributed data remain sparse in coverage. Future work needs to optimize multi-source cooperation strategies and leverage deep learning to enhance the robustness and global generalization of SM inversion.

5.3.2. Deep Learning and Physics-Guided Machine Learning—Improving Generalization and Interpretability

Machine learning, especially deep learning, increasingly appears in SM monitoring, often combined with physical priors such as radiative transfer models (RTMs) to boost accuracy [244,245]. For example, Singh & Gaurav in 2024 proposed a physics-informed neural network (PIML-SM) that incorporates an improved integral equation model into the loss function. Their model achieved an R of 0.94 and RMSE of 0.019 m^3/m^3 when using Sentinel-1/2 imagery [246]. Despite their success, these methods still face challenges: the limited representativeness of training samples, overfitting risks, and "black-box" behavior with weak interpretability. To address these, future research should incorporate strategies such as transfer learning, domain adaptation, physics-constrained networks, and uncertainty quantification (e.g., ensemble methods or Bayesian neural networks).

5.3.3. High-Order Radiative Transfer Models and Multi-Scale Roughness—Reducing Structural Bias

L-band signals are highly sensitive to vegetation structure and surface roughness. High-order RTMs that include multiple scattering mechanisms can more realistically estimate scattering, while multi-scale roughness parameterizations help reduce the biases inherent in empirical models [247]. For example, in 2023, Munoz-Martin et al. demonstrated that the precise modeling of surface roughness is critical for GNSS-R SM inversion:

roughness variations can induce tens of dB differences in reflectivity, significantly affecting retrieval errors [248]. Yet, deploying these models in practice is challenging because they require high-dimensional parameters (e.g., roughness spectra, 3D vegetation structure) that are difficult to measure directly. One method is to use high-fidelity RTMs in local regions to train machine learning models that can generalize these parameters to broader scales, thereby balancing physical realism with computational tractability.

5.3.4. SM Data Product Development via Multi-Source Fusion and AI—Toward Standardized, High-Resolution Products

The next generation of SM products is likely to emerge from the fusion of multi-sensor observations (e.g., GNSS-R, SAR, optical) and AI-optimized algorithms, yielding high-resolution, multi-scale, cross-regional, and standardized datasets. For example, Li et al. employed AutoML frameworks within a multi-sensor fusion architecture to build automated SM inversion models [245].

To further address the issue of regional inconsistency in data products, approaches that utilize fusion algorithms calibrated with physical models to generate refined downscaled datasets can be carried out. Additionally, an uncertainty quantification framework needs to be established to mitigate disparities in data validation scales, thereby ensuring both the precision and applicability of data products. Solutions may involve unified data formats (e.g., grid, temporal), physics model-calibrated fusion schemes, and hierarchical product structures that balance accuracy and applicability. Ultimately, by establishing systematic uncertainty frameworks and calibration procedures, these products can achieve both regional precision and applicability.

5.4. Key Challenges in Future

Looking ahead, several core challenges remain in SM monitoring:

The exploration of fusion technology of multi-source data and the establishment of uncertainty analysis frameworks for data evaluation standards

The interpretability and regional generalization of physics-guided ML models.

The practical deployment and validation of high-order RTMs and multi-scale parameterizations.

The development of standardized, high-resolution SM products through data assimilation and AI optimization.

Next-generation, high-quality L-band and multi-source observations are expected to provide the technical foundation to address these challenges, accelerating the construction of a more accurate, scalable, and globally applicable SM monitoring system.

6. Conclusions

Soil moisture, as a crucial variable in the hydrological cycle and energy balance, is a key component in water resource management, agricultural production, ecological protection, and disaster early warning. In recent years, advances in different approaches have significantly improved soil moisture monitoring, enabling large-scale, long-term, and multi-source observations and enhancing the understanding of land–atmosphere interactions. This review systematically surveyed the main soil moisture monitoring methods, including in situ measurements, optical and microwave remote sensing, thermodynamic and energy balance approaches, and methods based on radiation transfer models. In addition, the advantages and limitations of each method were analyzed and representative publicly available datasets were compared to provide research references and illustrate data diversity. Despite notable improvements in monitoring capability, challenges remain in complex environmental conditions, parameter uncertainty, and cross-regional applicability. Future research should focus on multi-source data integration, combining

physical models with machine learning, establishing a standardized validation principle, and developing cross-regional benchmarks to enhance product robustness and global applicability. Multi-source data fusion, deep learning optimization, and the construction of soil moisture data-sharing platforms will play key roles in improving accuracy and real-time monitoring.

Author Contributions: Conceptualization, methodology, formal analysis, investigation, and writing—original draft preparation, R.L.; data curation, S.L.; writing—review and editing, C.C. and R.Z.; project administration and funding acquisition, R.Z. All authors have read and agreed to the published version of the manuscript.

Funding: This work was supported by the Ministry of Science and Technology of the People's Republic of China (Third Xinjiang Scientific Expedition Program, Grant No. 2021xjkk0403), the National Natural Science Foundation of China (National Natural Science Foundation project, Grant No. 42071049), and the Xinjiang Tarim River Basin Authority, China (Project for Efficient Utilization of Water Resources in the Tarim River Basin, Grant No. TGJJG-2022KYXM0002).

Data Availability Statement: The data supporting this research was completely sourced from public repositories. Detailed references are provided in the manuscript.

Acknowledgments: The authors would like to thank all co-authors for their support and assistance in the preparation of this manuscript. Special appreciation is extended to Zhong Ruisen, for securing the financial support for this work. The authors are also grateful to the reviewers and editors for their valuable comments and constructive suggestions.

Conflicts of Interest: The authors declare that they have no known competing financial interests or personal relationships that could have appeared to influence the work reported in this paper.

Abbreviations

The following abbreviations are used in this manuscript:

SM	Soil Moisture
RS	Remote Sensing
RTM	Radiative Transfer Model
ET	Evapotranspiration
TDR	Time Domain Reflectometry
FDR	Frequency Domain Reflectometry
CIDR	Capacitance and Impedance Dielectric Reflectometry
GPR	Ground-Penetrating Radar
RFI	Radio-Frequency Interference
NMR	Nuclear Magnetic Resonance
CRNS	Cosmic Ray Neutron Probe
VTCI	Vegetation Temperature Condition Index
SWI	Soil Water Index
LST	Land Surface Temperature
VI	Vegetation Index
TVDI	Temperature Vegetation Drought Index
Ts	Temperature of the Surface
NDVI	Normalized Difference Vegetation Index
MPDI	Modified Perpendicular Drought Index
TIR	Thermal–Infrared Remote Sensing
ATI	Apparent Thermal Inertia
SEBAL	Surface Energy Balance Algorithm for Land
WCM	Water Cloud Model
RF	Random Forest

VOD	Vegetation Optical Depth
ACO	Ant Colony Optimization
SSA	Sparrow Search Algorithm
VMC	Vegetation Moisture Content
SCA	Single-Channel Algorithm
DCA	Dual-Channel Algorithm
CNN	Convolutional Neural Network
IEM	Integral Equation Model
S-CMCA	Spatially Constrained Multi-Channel Algorithm
Tb	Brightness Temperature
LSM	Land Surface Model

References

1. Saboori, M.; Ghag, K.S.; Panchanathan, A.; Patro, E.R.; Haghighi, A.T. Assessing feature importance for forecasting soil moisture in subarctic regions using gridded historical and forecasted climate data. *Geoderma* **2025**, *458*, 117304. [CrossRef]
2. Seneviratne, S.I.; Corti, T.; Davin, E.L.; Hirschi, M.; Jaeger, E.B.; Lehner, I.; Orlowsky, B.; Teuling, A.J. Investigating soil moisture–climate interactions in a changing climate: A review. *Earth-Sci. Rev.* **2010**, *99*, 125–161. [CrossRef]
3. Kasim, A.A.; Leng, P.; Li, Y.-X.; Liao, Q.-Y.; Geng, Y.J.; Ma, J.; Sun, Y.; Song, X.; Duan, S.-B.; Li, Z.-L. Remote sensing of root zone soil moisture: A review of methods and products. *J. Hydrol.* **2025**, *656*, 133002. [CrossRef]
4. Ivanova, I. Soil moisture forecasting from sensors-based soil moisture, weather and irrigation observations: A systematic review. *Smart Agric. Technol.* **2025**, *10*, 100692. [CrossRef]
5. Zha, X.; Zhu, W.; Han, Y.; Lv, A. Enhancing root-zone soil moisture estimation using Richards' equation and dynamic surface soil moisture data. *Agric. Water Manag.* **2025**, *312*, 109460. [CrossRef]
6. Susha Lekshmi, S.U.; Singh, D.N.; Shojaei Baghini, M. A critical review of soil moisture measurement. *Measurement* **2014**, *54*, 92–105. [CrossRef]
7. Wang, Q.; Xu, C.; Long, J.; Zhang, Q.; Luo, Y.; Li, L. Soil moisture deficits triggered by increasing compound drought and heat events during the growing season in Arid Central Asia. *J. Hydrol.* **2025**, *660*, 133397. [CrossRef]
8. Peng, J.; Albergel, C.; Balenzano, A.; Brocca, L.; Cartus, O.; Cosh, M.H.; Crow, W.T.; Dabrowska-Zielinska, K.; Dadson, S.; Davidson, M.W.J.; et al. A roadmap for high-resolution satellite soil moisture applications—Confronting product characteristics with user requirements. *Remote Sens. Environ.* **2021**, *252*, 112162. [CrossRef]
9. Mane, S.; Das, N.; Singh, G.; Cosh, M.; Dong, Y. Advancements in dielectric soil moisture sensor Calibration: A comprehensive review of methods and techniques. *Comput. Electron. Agric.* **2024**, *218*, 108686. [CrossRef]
10. Kim, H.; Wigneron, J.-P.; Kumar, S.; Dong, J.; Wagner, W.; Cosh, M.H.; Bosch, D.D.; Collins, C.H.; Starks, P.J.; Seyfried, M.; et al. Global scale error assessments of soil moisture estimates from microwave-based active and passive satellites and land surface models over forest and mixed irrigated/dryland agriculture regions. *Remote Sens. Environ.* **2020**, *251*, 112052. [CrossRef]
11. Zhang, D.; Zhou, G. Estimation of Soil Moisture from Optical and Thermal Remote Sensing: A Review. *Sensors* **2016**, *16*, 1308. [CrossRef] [PubMed]
12. Ho, T.K.; Feng, J.; Bilawal, F.; Shehab, S.H.; Trinh, K.T.; Yang, Y.; Rudiger, C.; Walker, J.P.; Karmakar, N.C. Lightweight and Compact Radiometers for Soil Moisture Measurement: A review. *IEEE Geosci. Remote Sens. Mag.* **2022**, *10*, 231–250. [CrossRef]
13. Liu, Y.; Yang, Y. Advances in the Quality of Global Soil Moisture Products: A Review. *Remote Sens.* **2022**, *14*, 3741. [CrossRef]
14. Babaeian, E.; Paheding, S.; Siddique, N.; Devabhaktuni, V.K.; Tuller, M. Estimation of root zone soil moisture from ground and remotely sensed soil information with multisensor data fusion and automated machine learning. *Remote Sens. Environ.* **2021**, *260*, 112434. [CrossRef]
15. Maya Moreshwar Meshram, S.; Adla, S.; Jourdin, L.; Pande, S. Review of low-cost, off-grid, biodegradable in situ autonomous soil moisture sensing systems: Is there a perfect solution? *Comput. Electron. Agric.* **2024**, *225*, 109289. [CrossRef]
16. Zhang, Q.; Kong, J.; Wang, L.; Zhong, Y. Estimating evapotranspiration using an improved two-source energy balance model coupled with soil moisture in arid and semi-arid regions. *J. Hydrol.* **2025**, *659*, 133283. [CrossRef]
17. Jiang, S.-H.; Yuan, Z.-R.; Wang, Z.Z.; Liu, X. Improved rainfall infiltration model for probabilistic slope stability assessment considering transition layers and spatial variability. *Eng. Geol.* **2025**, *353*, 108096. [CrossRef]
18. Baldwin, D.; Manfreda, S.; Keller, K.; Smithwick, E.A.H. Predicting root zone soil moisture with soil properties and satellite near-surface moisture data across the conterminous United States. *J. Hydrol.* **2017**, *546*, 393–404. [CrossRef]
19. Jiang, M.; Qiu, T.; Wang, T.; Zeng, C.; Zhang, B.; Shen, H. Seamless global daily soil moisture mapping using deep learning based spatiotemporal fusion. *Int. J. Appl. Earth Obs. Geoinf.* **2025**, *139*, 104517. [CrossRef]

20. Li, Z.; Yang, Q.; Li, J.; Jin, T.; Yuan, Q.; Shen, H.; Zhang, L. Global multi-scale surface soil moisture retrieval coupling physical mechanisms and machine learning in the cloud environment. *Remote Sens. Environ.* **2025**, *329*, 114928. [CrossRef]
21. Edokossi, K.; Calabia, A.; Jin, S.; Molina, I. GNSS-Reflectometry and Remote Sensing of Soil Moisture: A Review of Measurement Techniques, Methods, and Applications. *Remote Sens.* **2020**, *12*, 614. [CrossRef]
22. Yang, C.; Mao, K.; Guo, Z.; Shi, J.; Bateni, S.M.; Yuan, Z. Review of GNSS-R Technology for Soil Moisture Inversion. *Remote Sens.* **2024**, *16*, 1193. [CrossRef]
23. Lamichhane, M.; Mehan, S.; Mankin, K.R. Soil Moisture Prediction Using Remote Sensing and Machine Learning Algorithms: A Review on Progress, Challenges, and Opportunities. *Remote Sens.* **2025**, *17*, 2397. [CrossRef]
24. Senanayake, I.P.; Pathira Arachchilage, K.R.L.; Yeo, I.-Y.; Khaki, M.; Han, S.-C.; Dahlhaus, P.G. Spatial Downscaling of Satellite-Based Soil Moisture Products Using Machine Learning Techniques: A Review. *Remote Sens.* **2024**, *16*, 2067. [CrossRef]
25. Das, K.; Paul, P.K.; Dobesova, Z. Present status of soil moisture estimation by microwave remote sensing. *Cogent Geosci.* **2015**, *1*, 1084669. [CrossRef]
26. Kim, S.; Zhang, R.; Pham, H.; Sharma, A. A Review of Satellite-Derived Soil Moisture and Its Usage for Flood Estimation. *Remote Sens. Earth Syst. Sci.* **2019**, *2*, 225–246. [CrossRef]
27. Rasheed, M.W.; Tang, J.; Sarwar, A.; Shah, S.; Saddique, N.; Khan, M.U.; Imran Khan, M.; Nawaz, S.; Shamshiri, R.R.; Aziz, M.; et al. Soil Moisture Measuring Techniques and Factors Affecting the Moisture Dynamics: A Comprehensive Review. *Sustainability* **2022**, *14*, 11538. [CrossRef]
28. Yu, L.; Gao, W.; Shamshiri, R.R.; Tao, S.; Ren, Y.; Zhang, Y.; Su, G. Review of research progress on soil moisture sensor technology. *Int. J. Agric. Biol. Eng.* **2021**, *14*, 32–42. [CrossRef]
29. Chang, Z.; Zhang, F.; Xiong, J.; Ma, J.; Jin, B.; Zhang, D. Sensor-free Soil Moisture Sensing Using LoRa Signals. *Proc. ACM Interact. Mob. Wearable Ubiquitous Technol.* **2022**, *6*, 1–27. [CrossRef]
30. Dean, T.J.; Bell, J.P.; Baty, A.J.B. Soil-moisture measurement by an improved capacitance technique. *J. Hydrol.* **1987**, *93*, 67–78. [CrossRef]
31. Saleh, M.; Elhajj, I.H.; Asmar, D.; Bashour, I.; Kidess, S. Experimental Evaluation of Low-Cost Resistive Soil Moisture Sensors. In Proceedings of the 2016 IEEE International Multidisciplinary Conference on Engineering Technology (IMCET), Beirut, Lebanon, 2–4 November 2016; pp. 1–6. [CrossRef]
32. Bodasingi, V.K.; Rao, B.; Pillai, H.K. Laboratory Evaluation of a Low-Cost Soil Moisture and EC Sensor in Different Soil Types. *IEEE Trans. AgriFood Electron.* **2024**, *2*, 276–283. [CrossRef]
33. Robock, A.; Vinnikov, K.Y.; Srinivasan, G.; Entin, J.K.; HoIlinger, S.E.; Speranskaya, N.A.; Liu, S.; Namkhai, A. The global soil moisture data bank. *Bull. Am. Meteorol. Soc.* **2000**, *81*, 1281–1300. [CrossRef]
34. Gianessi, S.; Polo, M.; Stevanato, L.; Lunardon, M.; Ahmed, H.S.; Weltin, G.; Toloza, A.; Budach, C.; Biro, P.; Francke, T.; et al. Assessment of a new non-invasive soil moisture sensor based on cosmic-ray neutrons. In Proceedings of the 2021 IEEE International Workshop on Metrology for Agriculture and Forestry (MetroAgriFor), Trento-Bolzano, Italy, 3–5 November 2021; pp. 290–294.
35. Jones, S.B.; Wraith, J.M.; Or, D. Time domain reflectometry measurement principles and applications. *Hydrol. Process.* **2002**, *16*, 141–153. [CrossRef]
36. Tarantino, A.; Ridley, A.M.; Toll, D.G. Field Measurement of Suction, Water Content, and Water Permeability. *Geotech. Geol. Eng.* **2008**, *26*, 751–782. [CrossRef]
37. Nguyen, H.H.; Jeong, J.; Choi, M. Extension of cosmic-ray neutron probe measurement depth for improving field scale root-zone soil moisture estimation by coupling with representative in-situ sensors. *J. Hydrol.* **2019**, *571*, 679–696. [CrossRef]
38. Hannes, M.; Wollschläger, U.; Schrader, F.; Durner, W.; Gebler, S.; Pütz, T.; Fank, J.; von Unold, G.; Vogel, H.J. High-resolution estimation of the water balance components from high-precision lysimeters. *Hidrol. Earth System. Sci. Discuss.* **2015**, *12*, 569–608. [CrossRef]
39. Peters, A.; Nehls, T.; Schonsky, H.; Wessolek, G. Separating precipitation and evapotranspiration from noise—A new filter routine for high-resolution lysimeter data. *Hydrol. Earth Syst. Sci.* **2014**, *18*, 1189–1198. [CrossRef]
40. Huisman, J.A.; Sperl, C.; Bouten, W.; Verstraten, J.M. Soil Water Content Measurements at Different Scales Accuracy of Time. *J. Hydrol.* **2001**, *245*, 48–58. [CrossRef]
41. Qin, A.; Ning, D.; Liu, Z.; Duan, A.; Wang, J. Analysis of the Accuracy of an FDR Sensor in Soil Moisture Measurement under Laboratory and Field Conditions. *J. Sens.* **2021**, *2021*, 6665829. [CrossRef]
42. Petropoulos, G.P.; Ireland, G.; Barrett, B. Surface soil moisture retrievals from remote sensing: Current status, products & future trends. *Phys. Chem. Earth Parts A/B/C* **2015**, *83-84*, 36–56. [CrossRef]
43. Köhli, M.; Schrön, M.; Zreda, M.; Schmidt, U.; Dietrich, P.; Zacharias, S. Footprint characteristics revised for field-scale soil moisture monitoring with cosmic-ray neutrons. *Water Resour. Res.* **2015**, *51*, 5772–5790. [CrossRef]
44. Stevanato, L.; Baroni, G.; Cohen, Y.; Fontana, C.L.; Gatto, S.; Lunardon, M.; Marinello, F.; Moretto, S.; Morselli, L. A Novel Cosmic-Ray Neutron Sensor for Soil Moisture Estimation over Large Areas. *Agriculture* **2019**, *9*, 202. [CrossRef]

45. Magagi, R.; Berg, A.; Goïta, K.; Belair, S.; Jackson, T.; Toth, B.; Walker, A.; McNairn, H.; O'Neill, P.; Moghddam, M.; et al. Canadian Experiment for Soil Moisture in 2010 (CanEX-SM10): Overview and Preliminary Results. *IEEE Trans. Geosci. Remote Sens.* **2013**, *51*, 347–363. [CrossRef]
46. Djamai, N.; Magagi, R.; Goïta, K.; Hosseini, M.; Cosh, M.H.; Berg, A.; Toth, B. Evaluation of SMOS soil moisture products over the CanEx-SM10 area. *J. Hydrol.* **2015**, *520*, 254–267. [CrossRef]
47. Judge, J.; Liu, P.-W.; Monsiváis-Huertero, A.; Bongiovanni, T.; Chakrabarti, S.; Steele-Dunne, S.C.; Preston, D.; Allen, S.; Bermejo, J.P.; Rush, P.; et al. Impact of vegetation water content information on soil moisture retrievals in agricultural regions: An analysis based on the SMAPVEX16-MicroWEX dataset. *Remote Sens. Environ.* **2021**, *265*, 112623. [CrossRef]
48. Colliander, A.; Cosh, M.H.; Bourgeau-Chavez, L.; Kelly, V.R.; Kraatz, S.; Siqueira, P.; Walker, V.A.; Chen, X.; Roy, A.; Lakhankar, T.; et al. SMAP Validation Experiment 2019–2022 (SMAPVEX19–22): Field Campaign to Improve Soil Moisture and Vegetation Optical Depth Retrievals in Temperate Forests. *IEEE J. Sel. Top. Appl. Earth Obs. Remote Sens.* **2025**, *18*, 10749–10771. [CrossRef]
49. Panciera, R.; Walker, J.P.; Jackson, T.J.; Gray, D.A.; Tanase, M.A.; Ryu, D.; Monerris, A.; Yardley, H.; Rudiger, C.; Wu, X.; et al. The Soil Moisture Active Passive Experiments (SMAPEx): Toward Soil Moisture Retrieval From the SMAP Mission. *IEEE Trans. Geosci. Remote Sens.* **2014**, *52*, 490–507. [CrossRef]
50. Monsivais-Huertero, A.; Constantino-Recillas, D.E.; Hernandez-Sanchez, J.C.; Huerta-Batiz, H.E.; Judge, J.; Lopez-Estrada, P.A.; Jimenez-Escalona, J.C.; Arizmendi-Vasconcelos, E.; Garcia-Bernal, M.A.; Zambrano-Gallardo, C.F.; et al. Assessment of NASA SMAP Soil Moisture Products for Agricultural Regions in Central Mexico: An Analysis Based on the THEXMEX Dataset. *IEEE J. Sel. Top. Appl. Earth Obs. Remote Sens.* **2022**, *15*, 3421–3443. [CrossRef]
51. Galle, S.; Grippa, M.; Peugeot, C.; Moussa, I.B.; Cappelaere, B.; Demarty, J.; Mougin, E.; Panthou, G.; Adjomayi, P.; Agbossou, E.K.; et al. AMMA-CATCH, a Critical Zone Observatory in West Africa Monitoring a Region in Transition. *Vadose Zone J.* **2018**, *17*, 1–24. [CrossRef]
52. Rosnay, P.d.; Gruhier, C.; Timouk, F.; Baup, F.; Mougin, É.; Hiernaux, P.; Kergoat, L.; Dantec, V.L. Multi-scale soil moisture measurements at the Gourma meso-scale site in Mali. *J. Hydrol.* **2009**, *375*, 241–252. [CrossRef]
53. Dorigo, W.A.; Wagner, W.; Hohensinn, R.; Hahn, S.; Paulik, C.; Xaver, A.; Gruber, A.; Drusch, M.; Mecklenburg, S.; van Oevelen, P.; et al. The International Soil Moisture Network: A data hosting facility for global in situ soil moisture measurements. *Hydrol. Earth Syst. Sci.* **2011**, *15*, 1675–1698. [CrossRef]
54. Dorigo, W.; Himmelbauer, I.; Aberer, D.; Schremmer, L.; Petrakovic, I.; Zappa, L.; Preimesberger, W.; Xaver, A.; Annor, F.; Ardö, J.; et al. The International Soil Moisture Network: Serving Earth system science for over a decade. *Hydrol. Earth Syst. Sci.* **2021**, *25*, 5749–5804. [CrossRef]
55. Gruber, A.; De Lannoy, G.; Albergel, C.; Al-Yaari, A.; Brocca, L.; Calvet, J.C.; Colliander, A.; Cosh, M.; Crow, W.; Dorigo, W.; et al. Validation practices for satellite soil moisture retrievals: What are (the) errors? *Remote Sens. Environ.* **2020**, *244*, 111806. [CrossRef]
56. Sadeghi, M.; Babaeian, E.; Tuller, M.; Jones, S.B. The optical trapezoid model: A novel approach to remote sensing of soil moisture applied to Sentinel-2 and Landsat-8 observations. *Remote Sens. Environ.* **2017**, *198*, 52–68. [CrossRef]
57. Du, R.; Xiang, Y.; Zhang, F.; Chen, J.; Shi, H.; Liu, H.; Yang, X.; Yang, N.; Yang, X.; Wang, T.; et al. Combing transfer learning with the OPtical TRApezoid Model (OPTRAM) to diagnosis small-scale field soil moisture from hyperspectral data. *Agric. Water Manag.* **2024**, *298*, 108856. [CrossRef]
58. Hao, Y.; Baik, J.; Choi, M. Developing a soil water index-based Priestley–Taylor algorithm for estimating evapotranspiration over East Asia and Australia. *Agric. For. Meteorol.* **2019**, *279*, 107760. [CrossRef]
59. Paulik, C.; Dorigo, W.; Wagner, W.; Kidd, R. Validation of the ASCAT Soil Water Index using in situ data from the International Soil Moisture Network. *Int. J. Appl. Earth Obs. Geoinf.* **2014**, *30*, 1–8. [CrossRef]
60. Zhao, D.; Kuenzer, C.; Fu, C.; Wagner, W. Evaluation of the ERS Scatterometer-Derived Soil Water Index to Monitor Water Availability and Precipitation Distribution at Three Different Scales in China. *J. Hydrometeorol.* **2008**, *9*, 549–562. [CrossRef]
61. Wagner, W.; Lemoine, G.; Rott, H. A Method for Estimating Soil Moisture from ERS Scatterometer and Soil Data. *Remote Sens. Environ.* **1999**, *70*, 191–207. [CrossRef]
62. Fathololoumi, S.; Karimi Firozjaei, M.; Biswas, A. Improving spatial resolution of satellite soil water index (SWI) maps under clear-sky conditions using a machine learning approach. *J. Hydrol.* **2022**, *615*, 128709. [CrossRef]
63. Merabti, A.; Darouich, H.; Paredes, P.; Meddi, M.; Pereira, L.S. Assessing Spatial Variability and Trends of Droughts in Eastern Algeria Using SPI, RDI, PDSI, and MedPDSI—A Novel Drought Index Using the FAO56 Evapotranspiration Method. *Water* **2023**, *15*, 626. [CrossRef]
64. Dash, S.K.; Sembhi, H.; Langsdale, M.; Wooster, M.; Dodd, E.; Ghent, D.; Sinha, R. Assessing the field-scale crop water condition over an intensive agricultural plain using UAV-based thermal and multispectral imagery. *J. Hydrol.* **2025**, *655*, 132966. [CrossRef]
65. Peng, J.; Loew, A.; Zhang, S.; Wang, J.; Niesel, J. Spatial Downscaling of Satellite Soil Moisture Data Using a Vegetation Temperature Condition Index. *IEEE Trans. Geosci. Remote Sens.* **2016**, *54*, 558–566. [CrossRef]

66. Wang, P.X.; Li, X.W.; Gong, J.Y.; Song, C. Vegetation Temperature Condition Index and Its Application for Drought Monitoring. In Proceedings of the IGARSS 2001. Scanning the Present and Resolving the Future. Proceedings. IEEE 2001 International Geoscience and Remote Sensing Symposium (Cat. No.01CH37217), Sydney, NSW, Australia, 9–13 July 2001; pp. 141–143.
67. Wan, Z.; Wang, P.; Li, X. Using MODIS Land Surface Temperature and Normalized Difference Vegetation Index products for monitoring drought in the southern Great Plains, USA. *Int. J. Remote Sens.* **2010**, *25*, 61–72. [CrossRef]
68. Tian, H.; Wang, P.; Tansey, K.; Han, D.; Zhang, J.; Zhang, S.; Li, H. A deep learning framework under attention mechanism for wheat yield estimation using remotely sensed indices in the Guanzhong Plain, PR China. *Int. J. Appl. Earth Obs. Geoinf.* **2021**, *102*, 102375. [CrossRef]
69. Carlson, T.N. Triangle Models and Misconceptions. *Int. J. Remote Sens. Appl.* **2013**, *3*, 155–158.
70. Cai, J.; Zhao, W.; Ding, T.; Yin, G. Generation of High-Resolution Surface Soil Moisture over Mountain Areas by Spatially Downscaling Remote Sensing Products Based on Land Surface Temperature–Vegetation Index Feature Space. *J. Remote Sens.* **2025**, *5*, 1–18. [CrossRef]
71. Tang, R.; Li, Z.-L.; Liu, M.; Jiang, Y.; Peng, Z. A moisture-based triangle approach for estimating surface evaporative fraction with time-series of remotely sensed data. *Remote Sens. Environ.* **2022**, *280*, 113212. [CrossRef]
72. Leng, P.; Li, Z.-L.; Liao, Q.-Y.; Ma, J.; Sun, Y.; Song, Q.; Zhang, X.; Shang, G.-F. Trapezoid-based surface soil moisture retrieval using a pixel-to-pixel scheme: A preliminary result over the North China Plain. *J. Hydrol.* **2022**, *613*, 128350. [CrossRef]
73. He, L.; Cheng, Y.; Li, Y.; Li, F.; Fan, K.; Li, Y. An Improved Method for Soil Moisture Monitoring with Ensemble Learning Methods Over the Tibetan Plateau. *IEEE J. Sel. Top. Appl. Earth Obs. Remote Sens.* **2021**, *14*, 2833–2844. [CrossRef]
74. Sandholt, I.; Rasmussen, K.; Andersen, J. A simple interpretation of the surface temperature/vegetation index space for assessment of surface moisture status. *Remote Sens. Environ.* **2002**, *79*, 213–224. [CrossRef]
75. Huang, D.; Ma, T.; Liu, J.; Zhang, J. Agricultural drought monitoring using modified TVDI and dynamic drought thresholds in the upper and middle Huai River Basin, China. *J. Hydrol. Reg. Stud.* **2025**, *57*, 102069. [CrossRef]
76. Bian, Z.; Roujean, J.L.; Fan, T.; Dong, Y.; Hu, T.; Cao, B.; Li, H.; Du, Y.; Xiao, Q.; Liu, Q. An angular normalization method for temperature vegetation dryness index (TVDI) in monitoring agricultural drought. *Remote Sens. Environ.* **2023**, *284*, 113330. [CrossRef]
77. Guo, Y.; Han, L.; Zhang, D.; Sun, G.; Fan, J.; Ren, X. The Factors Affecting the Quality of the Temperature Vegetation Dryness Index (TVDI) and the Spatial–Temporal Variations in Drought from 2011 to 2020 in Regions Affected by Climate Change. *Sustainability* **2023**, *15*, 11350. [CrossRef]
78. Meng, M.; Jian, N.; Zhi-Guo, Z. Aridity Index and Its Applications in Geo-Ecological Study. *Chin. J. Plant Ecol.* **2003**, *28*, 853–861. [CrossRef]
79. Spinoni, J.; Vogt, J.; Naumann, G.; Carrao, H.; Barbosa, P. Towards identifying areas at climatological risk of desertification using the Köppen-Geiger classification and FAO aridity index. *Int. J. Climatol.* **2015**, *35*, 2210–2222. [CrossRef]
80. Lu, J.; Yao, L.; Qin, J.; Jiang, H.; Zhou, C. Global reconstruction of gridded aridity index and its spatial and temporal characterization from 2003 to 2022. *Int. J. Digit. Earth* **2025**, *18*, 2473639. [CrossRef]
81. Yao, P.; Lu, H.; Zhao, T.; Wu, S.; Peng, Z.; Cosh, M.H.; Jia, L.; Yang, K.; Zhang, P.; Shi, J. A global daily soil moisture dataset derived from Chinese FengYun Microwave Radiation Imager (MWRI) (2010–2019). *Sci. Data* **2023**, *10*, 133. [CrossRef]
82. Jackson, R.D.; Idso, S.B.; Reginato, R.J.; Pinter, P.J., Jr. Canopy temperature as a crop water stress indicator. *Water Resour. Res.* **1981**, *17*, 1133–1138. [CrossRef]
83. Jackson, R.D.; Kustas, W.P.; Choudhury, B.J. A reexamination of the crop water stress index. *Irrig. Sci.* **1988**, *9*, 309–317. [CrossRef]
84. Idso, S.B.; Reginato, R.J.; Radin, J.W. Leaf diffusion resistance and photosynthesis in cotton as related to a foliage temperature based plant water stress index. *Agric. Meteorol.* **1982**, *27*, 27–34. [CrossRef]
85. Amani, M.; Parsian, S.; MirMazloumi, S.M.; Aieneh, O. Two new soil moisture indices based on the NIR-red triangle space of Landsat-8 data. *Int. J. Appl. Earth Obs. Geoinf.* **2016**, *50*, 176–186. [CrossRef]
86. Moran, M.S.; Clarke, T.R.; Inoue, Y.; Vidal, A. Estimating crop water deficit using the relation between surface-air temperature and spectral vegetation index. *Remote Sens. Environ.* **1994**, *49*, 246–263. [CrossRef]
87. Fensholt, R.; Sandholt, I. Derivation of a shortwave infrared water stress index from MODIS near- and shortwave infrared data in a semiarid environment. *Remote Sens. Environ.* **2003**, *87*, 111–121. [CrossRef]
88. Ghulam, A.; Qin, Q.; Wang, L.; Zhan, Z.; Wang, D. Development of broadband albedo based ecological safety monitoring index. In Proceedings of the IGARSS 2004. 2004 IEEE International Geoscience and Remote Sensing Symposium, Anchorage, AK, USA, 20–24 September 2004; pp. 4115–4118. [CrossRef]
89. Ghulam, A.; Qin, Q.; Teyip, T.; Li, Z.-L. Modified perpendicular drought index (MPDI): A real-time drought monitoring method. *ISPRS J. Photogramm. Remote Sens.* **2007**, *62*, 150–164. [CrossRef]
90. Kogan, F.N. Droughts of the late 1980s in the United States as derived from NOAA polar-orbiting satellite data. *Bull. Am. Meteorol. Soc.* **1995**, *76*, 655–668. [CrossRef]

91. Kogan, F.N. Remote sensing of weather impacts on vegetation in non-homogeneous areas. *Int. J. Remote Sens.* **2007**, *11*, 1405–1419. [CrossRef]
92. Shi, H.; Liu, Z.; Li, S.; Jin, M.; Tang, Z.; Sun, T.; Liu, X.; Li, Z.; Zhang, F.; Xiang, Y. Monitoring Soybean Soil Moisture Content Based on UAV Multispectral and Thermal-Infrared Remote-Sensing Information Fusion. *Plants* **2024**, *13*, 2417. [CrossRef]
93. Liu, Y.; Qian, J.; Yue, H. Comprehensive Evaluation of Sentinel-2 Red Edge and Shortwave-Infrared Bands to Estimate Soil Moisture. *IEEE J. Sel. Top. Appl. Earth Obs. Remote Sens.* **2021**, *14*, 7448–7465. [CrossRef]
94. Price, J.C. On the Analysis of Thermal Infrared Imagery: The Limited Utility of Apparent Thermal Inertia. *Remote Sens. Environ.* **1985**, *73*, 59–73. [CrossRef]
95. Lu, Y.; Horton, R.; Zhang, X.; Ren, T. Accounting for soil porosity improves a thermal inertia model for estimating surface soil water content. *Remote Sens. Environ.* **2018**, *212*, 79–89. [CrossRef]
96. Lu, S.; Ju, Z.; Ren, T.; Horton, R. A general approach to estimate soil water content from thermal inertia. *Agric. For. Meteorol.* **2009**, *149*, 1693–1698. [CrossRef]
97. Wienhold, K.J.; Li, D.; Fang, Z.N. Precision Irrigation Soil Moisture Mapper: A Thermal Inertia Approach to Estimating Volumetric Soil Water Content Using Unmanned Aerial Vehicles and Multispectral Imagery. *Remote Sens.* **2024**, *16*, 1660. [CrossRef]
98. Awada, H.; Sirca, C.; Marras, S.; Castellini, M.; Spano, D.; Pirastru, M. Modelling soil moisture and daily actual evapotranspiration: Integrating remote sensing surface energy balance and 1D Richards equation. *Int. J. Appl. Earth Obs. Geoinf.* **2024**, *128*, 103744. [CrossRef]
99. Pang, Z.; Hua, D.; Li, J.; Li, J. Temporal variation and environmental drivers of soil heat flux and surface solar radiation in the northern Qinling foothills. *Front. Environ. Sci.* **2025**, *13*, 1594923. [CrossRef]
100. Araya, S.N.; Fryjoff-Hung, A.; Anderson, A.; Viers, J.H.; Ghezzehei, T.A. Advances in soil moisture retrieval from multispectral remote sensing using unoccupied aircraft systems and machine learning techniques. *Hydrol. Earth Syst. Sci.* **2021**, *25*, 2739–2758. [CrossRef]
101. Uebbing, B.; Forootan, E.; Braakmann-Folgmann, A.; Kusche, J. Inverting surface soil moisture information from satellite altimetry over arid and semi-arid regions. *Remote Sens. Environ.* **2017**, *196*, 205–223. [CrossRef]
102. Njoku, E.; Chan, S. Soil Moisture from the Advanced Microwave Scanning Radiometer (AMSR) Instruments. *Compr. Remote Sens.* **2018**, *4*, 191–223. [CrossRef]
103. Singh, D. Effect of soil moisture on microwave scattering for remote sensing. *Sadhan* **1999**, *24*, 485–493. [CrossRef]
104. Gao, Y.; Colliander, A.; Burgin, M.S.; Walker, J.P.; Dinnat, E.; Chae, C.; Cosh, M.H.; Caldwell, T.G.; Berg, A.; Martinez-Fernandez, J.; et al. Multi-frequency radiometer-based soil moisture retrieval and algorithm parameterization using in situ sites. *Remote Sens. Environ.* **2022**, *279*, 113113. [CrossRef]
105. Li, T.; Hajnsek, I.; Chen, K.-S. Sensitivity Analysis of Bistatic Scattering for Soil Moisture Retrieval. *Remote Sens.* **2021**, *13*, 188. [CrossRef]
106. De Jeu, R.; Malbeteau, Y.; Zotta, R.-M.; Dorigo, W.; Wu, X.; Walker, J.; Miralles, D.G. Analyzing satellite and airborne Ka-band passive microwave observations over land for temperature and vegetation monitoring. *Front. Remote Sens.* **2025**, *6*, 1574072. [CrossRef]
107. Holmes, T.R.H.; De Jeu, R.A.M.; Owe, M.; Dolman, A.J. Land surface temperature from Ka band (37 GHz) passive microwave observations. *J. Geophys. Res. Atmos.* **2009**, *114*, D04113. [CrossRef]
108. Anconitano, G.; Kim, S.-B. Sensitivity to soil moisture of Capella X-band high-resolution SAR data over forests. *Sci. Remote Sens.* **2025**, *12*, 100289. [CrossRef]
109. Ulaby, F.; Long, D.; Blackwell, W.; Elachi, C.; Fung, A.; Ruf, C.; Sarabandi, K.; Zebker, H.; Van Zyl, J. *Microwave Radar and Radiometric Remote Sensing*; University of Michigan Press: Ann Arbor, MI, USA, 2014; pp. 45–47.
110. Kerr, Y.H.; Waldteufel, P.; Wigneron, J.-P.; Delwart, S.; Cabot, F.; Boutin, J.; Escorihuela, M.-J.; Font, J.; Reul, N.; Gruhier, C.; et al. The SMOS Mission: New Tool for Monitoring Key Elements ofthe Global Water Cycle. *Proc. IEEE* **2010**, *98*, 666–687. [CrossRef]
111. Entekhabi, D.; Njoku, E.G.; O'Neill, P.E.; Kellogg, K.H.; Crow, W.T.; Edelstein, W.N.; Entin, J.K.; Goodman, S.D.; Jackson, T.J.; Johnson, J.; et al. The Soil Moisture Active Passive (SMAP) Mission. *Proc. IEEE* **2010**, *98*, 704–716. [CrossRef]
112. Bauer-Marschallinger, B.; Freeman, V.; Cao, S.; Paulik, C.; Schaufler, S.; Stachl, T.; Modanesi, S.; Massari, C.; Ciabatta, L.; Brocca, L.; et al. Toward Global Soil Moisture Monitoring with Sentinel-1: Harnessing Assets and Overcoming Obstacles. *IEEE Trans. Geosci. Remote Sens.* **2019**, *57*, 520–539. [CrossRef]
113. Rana, D.; Mazzanti, P.; Bozzano, F. Estimation of High-Resolution Soil Moisture from Dual Frequency Synthetic Aperture Radar (SAOCOM L-Band & Sentinel-1 C-Band) dataset in the Petacciato landslide area, Italy. In Proceedings of the EUSAR 2024–15th European Conference on Synthetic Aperture Radar, Munich, Germany, 23–26 April 2024; pp. 287–392.
114. Xing, Z.; Zhao, L.; Fan, L.; De Lannoy, G.; Bai, X.; Liu, X.; Peng, J.; Frappart, F.; Yang, K.; Li, X.; et al. Retrieval of 1 km surface soil moisture from Sentinel-1 over bare soil and grassland on the Qinghai-Tibetan Plateau. *Remote Sens. Environ.* **2025**, *318*, 114563. [CrossRef]

115. Fan, D.; Zhao, T.; Jiang, X.; García-García, A.; Schmidt, T.; Samaniego, L.; Attinger, S.; Wu, H.; Jiang, Y.; Shi, J.; et al. A Sentinel-1 SAR-based global 1-km resolution soil moisture data product: Algorithm and preliminary assessment. *Remote Sens. Environ.* **2025**, *318*, 114579. [CrossRef]
116. Wu, Z.; Cui, N.; Zhang, W.; Gong, D.; Liu, C.; Liu, Q.; Zheng, S.; Wang, Z.; Zhao, L.; Yang, Y. Inversion of large-scale citrus soil moisture using multi-temporal Sentinel-1 and Landsat-8 data. *Agric. Water Manag.* **2024**, *294*, 108718. [CrossRef]
117. Han, L.; Wang, C.; Yu, T.; Gu, X.; Liu, Q. High-Precision Soil Moisture Mapping Based on Multi-Model Coupling and Background Knowledge, Over Vegetated Areas Using Chinese GF-3 and GF-1 Satellite Data. *Remote Sens.* **2020**, *12*, 2123. [CrossRef]
118. Quast, R.; Wagner, W.; Bauer-Marschallinger, B.; Vreugdenhil, M. Soil moisture retrieval from Sentinel-1 using a first-order radiative transfer model—A case-study over the Po-Valley. *Remote Sens. Environ.* **2023**, *295*, 113651. [CrossRef]
119. Tabatabaeenejad, A.; Chen, R.H.; Burgin, M.S.; Duan, X.; Cuenca, R.H.; Cosh, M.H.; Scott, R.L.; Moghaddam, M. Assessment and Validation of AirMOSS P-Band Root-Zone Soil Moisture Products. *IEEE Trans. Geosci. Remote Sens.* **2020**, *58*, 6181–6196. [CrossRef]
120. Martens, B.; Lievens, H.; Colliander, A.; Jackson, T.J.; Verhoest, N.E.C. Estimating Effective Roughness Parameters of the L-MEB Model for Soil Moisture Retrieval Using Passive Microwave Observations from SMAPVEX12. *IEEE Trans. Geosci. Remote Sens.* **2015**, *53*, 4091–4103. [CrossRef]
121. Cui, K.; Xing, M.; Shang, J.; Zhou, X.; Wang, J. Enhanced L-MEB Model for Soil Moisture Retrieval Over Soybean Fields During the Growing Season. *IEEE Trans. Geosci. Remote Sens.* **2025**, *63*, 4409216. [CrossRef]
122. Wang, Z.; Che, T.; Liou, Y.-A. Global Sensitivity Analysis of the L-MEB Model for Retrieving Soil Moisture. *IEEE Trans. Geosci. Remote Sens.* **2016**, *54*, 2949–2962. [CrossRef]
123. Yi, C.; Li, X.; Zeng, J.; Fan, L.; Xie, Z.; Gao, L.; Xing, Z.; Ma, H.; Boudah, A.; Zhou, H.; et al. Assessment of five SMAP soil moisture products using ISMN ground-based measurements over varied environmental conditions. *J. Hydrol.* **2023**, *619*, 129325. [CrossRef]
124. Li, X.; Wigneron, J.-P.; Fan, L.; Frappart, F.; Yueh, S.H.; Colliander, A.; Ebtehaj, A.; Gao, L.; Fernandez-Moran, R.; Liu, X.; et al. A new SMAP soil moisture and vegetation optical depth product (SMAP-IB): Algorithm, assessment and inter-comparison. *Remote Sens. Environ.* **2022**, *271*, 112921. [CrossRef]
125. Sharma, J.; Prasad, R.; Srivastava, P.K.; Singh, S.K.; Yadav, S.A.; Pandey, D.K. Improved radar vegetation water content integration for SMAP soil moisture retrieval. *Remote Sens. Appl. Soc. Environ.* **2025**, *37*, 101443. [CrossRef]
126. Gao, L.; Ebtehaj, A.; Chaubell, M.J.; Sadeghi, M.; Li, X.; Wigneron, J.-P. Reappraisal of SMAP inversion algorithms for soil moisture and vegetation optical depth. *Remote Sens. Environ.* **2021**, *264*, 112627. [CrossRef]
127. Chaubell, M.J.; Yueh, S.H.; Dunbar, R.S.; Colliander, A.; Chen, F.; Chan, S.K.; Entekhabi, D.; Bindlish, R.; O'Neill, P.E.; Asanuma, J.; et al. Improved SMAP Dual-Channel Algorithm for the Retrieval of Soil Moisture. *IEEE Trans. Geosci. Remote Sens.* **2020**, *58*, 3894–3905. [CrossRef]
128. Crow, W.T.; Feldman, A.F. Vegetation signal crosstalk present in official SMAP surface soil moisture retrievals. *Remote Sens. Environ.* **2025**, *316*, 114466. [CrossRef]
129. Wigneron, J.-P.; Li, X.; Frappart, F.; Fan, L.; Al-Yaari, A.; De Lannoy, G.; Liu, X.; Wang, M.; Le Masson, E.; Moisy, C. SMOS-IC data record of soil moisture and L-VOD: Historical development, applications and perspectives. *Remote Sens. Environ.* **2021**, *254*, 112238. [CrossRef]
130. Lee, J.H.; Pellarin, T.; Kerr, Y.H. Inversion of soil hydraulic properties from the DEnKF analysis of SMOS soil moisture over West Africa. *Agric. For. Meteorol.* **2014**, *188*, 76–88. [CrossRef]
131. Román-Cascón, C.; Pellarin, T.; Gibon, F.; Brocca, L.; Cosme, E.; Crow, W.; Fernández-Prieto, D.; Kerr, Y.H.; Massari, C. Correcting satellite-based precipitation products through SMOS soil moisture data assimilation in two land-surface models of different complexity: API and SURFEX. *Remote Sens. Environ.* **2017**, *200*, 295–310. [CrossRef]
132. Li, Y.; Zhu, M.; Luo, L.; Wang, S.; Chen, C.; Zhang, Z.; Yao, Y.; Hu, X. GNSS-IR dual-frequency data fusion for soil moisture inversion based on Helmert variance component estimation. *J. Hydrol.* **2024**, *631*, 130752. [CrossRef]
133. Li, Y.; Xu, T.; Yang, S.; Yu, K.; Chang, X.; Jin, T. A Forward Model and Inversion Algorithm for Near-Surface Soil Moisture Estimation with GNSS Refraction Pattern Technique. *IEEE Trans. Geosci. Remote Sens.* **2024**, *62*, 4301119. [CrossRef]
134. Zhang, R.; Chan, S.; Bindlish, R.; Lakshmi, V. A Performance Analysis of Soil Dielectric Models over Organic Soils in Alaska for Passive Microwave Remote Sensing of Soil Moisture. *Remote Sens.* **2023**, *15*, 1658. [CrossRef]
135. Srivastava, P.K.; O'Neill, P.; Cosh, M.; Kurum, M.; Lang, R.; Joseph, A. Evaluation of Dielectric Mixing Models for Passive Microwave Soil Moisture Retrieval Using Data from ComRAD Ground-Based SMAP Simulator. *IEEE J. Sel. Top. Appl. Earth Obs. Remote Sens.* **2015**, *8*, 4345–4354. [CrossRef]
136. Mialon, A.; Richaume, P.; Leroux, D.; Bircher, S.; Bitar, A.A.; Pellarin, T.; Wigneron, J.-P.; Kerr, Y.H. Comparison of Dobson and Mironov Dielectric Models in the SMOS Soil Moisture Retrieval Algorithm. *IEEE Trans. Geosci. Remote Sens.* **2015**, *53*, 3084–3094. [CrossRef]
137. Suman, S.; Srivastava, P.K.; Pandey, D.K.; Prasad, R.; Mall, R.K.; O'Neill, P. Comparison of soil dielectric mixing models for soil moisture retrieval using SMAP brightness temperature over croplands in India. *J. Hydrol.* **2021**, *602*, 126673. [CrossRef]

138. Sawada, Y.; Koike, T.; Aida, K.; Toride, K.; Walker, J.P. Fusing Microwave and Optical Satellite Observations to Simultaneously Retrieve Surface Soil Moisture, Vegetation Water Content, and Surface Soil Roughness. *IEEE Trans. Geosci. Remote Sens.* **2017**, *55*, 6195–6206. [CrossRef]
139. Liu, J.; Liu, Q. Soil Moisture Estimate Uncertainties from the Effect of Soil Texture on Dielectric Semiempirical Models. *Remote Sens.* **2020**, *12*, 2343. [CrossRef]
140. Gao, L.; Song, X.; Li, X.; Ma, J.; Leng, P.; Wang, W.; Zhu, X. An Enhanced Saline Soil Dielectric Constant Model Used for Remote Sensing Soil Moisture and Salinity Retrieval. *Remote Sens.* **2024**, *16*, 452. [CrossRef]
141. Escorihuela, M.J.; Kerr, Y.H.; de Rosnay, P.; Wigneron, J.P.; Calvet, J.C.; Lemaitre, F. A Simple Model of the Bare Soil Microwave Emission at L-Band. *IEEE Trans. Geosci. Remote Sens.* **2007**, *45*, 1978–1987. [CrossRef]
142. Walker, V.A.; Wallace, V.; Yildirim, E.; Eichinger, W.E.; Cosh, M.H.; Hornbuckle, B.K. From field observations to temporally dynamic soil surface roughness retrievals in the U.S. Corn Belt. *Remote Sens. Environ.* **2023**, *287*, 113458. [CrossRef]
143. Neelam, M.; Colliander, A.; Mohanty, B.P.; Cosh, M.H.; Misra, S.; Jackson, T.J. Multiscale Surface Roughness for Improved Soil Moisture Estimation. *IEEE Trans. Geosci. Remote Sens.* **2020**, *58*, 5264–5276. [CrossRef]
144. Yin, Q.; Li, J.; Ma, F.; Xiang, D.; Zhang, F. Dual-Channel Convolutional Neural Network for Bare Surface Soil Moisture Inversion Based on Polarimetric Scattering Models. *Remote Sens.* **2021**, *13*, 4503. [CrossRef]
145. Konkathi, P.; Li, X.; Fernandez-Moran, R.; Liu, X.; Xing, Z.; Frappart, F.; Piles, M.; Karthikeyan, L.; Wigneron, J.-P. A novel calibration of global soil roughness effects for SMOS-IC soil moisture and L-VOD products. *Remote Sens. Environ.* **2025**, *329*, 114946. [CrossRef]
146. Lee, J.H.; Kim, H.-C. The Impact of Sentinel-1-Corrected Fractal Roughness on Soil Moisture Retrievals. *Fractal Fract.* **2024**, *8*, 137. [CrossRef]
147. Kim, S.-B.; Huang, H.; Liao, T.-H.; Colliander, A. Estimating Vegetation Water Content and Soil Surface Roughness Using Physical Models of L-Band Radar Scattering for Soil Moisture Retrieval. *Remote Sens.* **2018**, *10*, 556. [CrossRef]
148. Gao, L.; Sadeghi, M.; Feldman, A.F.; Ebtehaj, A. A Spatially Constrained Multichannel Algorithm for Inversion of a First-Order Microwave Emission Model at L-Band. *IEEE Trans. Geosci. Remote Sens.* **2020**, *58*, 8134–8146. [CrossRef]
149. Zhang, R.; Watts, A.C.; Alipour, M. Inverse Dynamic Parameter Identification for Remote Sensing of Soil Moisture from SMAP Satellite Observations. *IEEE J. Sel. Top. Appl. Earth Obs. Remote Sens.* **2024**, *17*, 16592–16607. [CrossRef]
150. Li, X.; Al-Yaari, A.; Schwank, M.; Fan, L.; Frappart, F.; Swenson, J.; Wigneron, J.P. Compared performances of SMOS-IC soil moisture and vegetation optical depth retrievals based on Tau-Omega and Two-Stream microwave emission models. *Remote Sens. Environ.* **2020**, *236*, 111502. [CrossRef]
151. Shen, X.; Walker, J.P.; Ye, N.; Wu, X.; Brakhasi, F.; Boopathi, N.; Zhu, L.; Yeo, I.-Y.; Kim, E.; Kerr, Y.; et al. Evaluation of the tau-omega model over bare and wheat-covered flat and periodic soil surfaces at P- and L-band. *Remote Sens. Environ.* **2022**, *273*, 112960. [CrossRef]
152. Park, C.-H.; Jagdhuber, T.; Colliander, A.; Lee, J.; Berg, A.; Cosh, M.; Kim, S.-B.; Kim, Y.; Wulfmeyer, V. Parameterization of Vegetation Scattering Albedo in the Tau-Omega Model for Soil Moisture Retrieval on Croplands. *Remote Sens.* **2020**, *12*, 2939. [CrossRef]
153. Park, C.-H.; Jagdhuber, T.; Colliander, A.; Berg, A.; Cosh, M.H.; Lee, J.; Boo, K.-O. Retrieving forest soil moisture from SMAP observations considering a microwave polarization difference index (MPDI) to -ω model. *Sci. Remote Sens.* **2024**, *9*, 100131. [CrossRef]
154. FUJII, H.; KOIKE, T.; IMAOKA, K. Improvement of the AMSR-E Algorithm for Soil Moisture Estimation by Introducing a Fractional Vegetation Coverage Dataset Derived from MODIS Data. *J. Remote Sens. Soc. Jpn.* **2009**, *29*, 282–292. [CrossRef]
155. Njoku, E.G.; Jackson, T.J.; Lakshmi, V.; Chan, T.K.; Nghiem, S.V. Soil moisture retrieval from AMSR-E. *IEEE Trans. Geosci. Remote Sens.* **2003**, *41*, 215–229. [CrossRef]
156. Owe, M.; de Jeu, R.; Holmes, T. Multisensor historical climatology of satellite-derived global land surface moisture. *J. Geophys. Res. Earth Surf.* **2008**, *113*, F01002. [CrossRef]
157. Jackson, T.; Chan, S.; Bindlish, R.; Njoku, E. *AMSR-E/AMSR2 Unified L2B Half-Orbit 25 km EASE-Grid Surface Soil Moisture, Version 1*; National Snow and Ice Data Center (NSIDC): Boulder, CO, USA, 2018. [CrossRef]
158. Cho, E.; Su, C.-H.; Ryu, D.; Kim, H.; Choi, M. Does AMSR2 produce better soil moisture retrievals than AMSR-E over Australia? *Remote Sens. Environ.* **2017**, *188*, 95–105. [CrossRef]
159. Hu, L.; Zhao, T.; Ju, W.; Peng, Z.; Shi, J.; Rodríguez-Fernández, N.J.; Wigneron, J.-P.; Cosh, M.H.; Yang, K.; Lu, H.; et al. A twenty-year dataset of soil moisture and vegetation optical depth from AMSR-E/2 measurements using the multi-channel collaborative algorithm. *Remote Sens. Environ.* **2023**, *292*, 113595. [CrossRef]
160. Yao, P.; Lu, H.; Shi, J.; Zhao, T.; Yang, K.; Cosh, M.H.; Gianotti, D.J.S.; Entekhabi, D. A long term global daily soil moisture dataset derived from AMSR-E and AMSR2 (2002-2019). *Sci. Data* **2021**, *8*, 143. [CrossRef] [PubMed]
161. Song, P.; Zhang, Y.; Guo, J.; Shi, J.; Zhao, T.; Tong, B. A 1-km daily surface soil moisture dataset of enhanced coverage under all-weather conditions over China in 2003-2019. *Earth Syst. Sci. Data* **2022**, *14*, 2613–2637. [CrossRef]

162. Bindlish, R.; Jackson, T.; Cosh, M.; Zhao, T.; O'Neill, P. Global soil moisture from the Aquarius/SAC-D satellite: Description and initial assessment. *IEEE Geosci. Remote Sens. Lett.* **2015**, *12*, 923–927. [CrossRef]
163. Wagner, W.; Hahn, S.; Kidd, R.; Melzer, T.; Bartalis, Z.; Hasenauer, S.; Figa-Saldaña, J.; de Rosnay, P.; Jann, A.; Schneider, S.; et al. The ASCAT Soil Moisture Product: A Review of its Specifications, Validation Results, and Emerging Applications. *Meteorol. Z.* **2013**, *22*, 5–33. [CrossRef]
164. Bartalis, Z.; Wagner, W.; Naeimi, V.; Hasenauer, S.; Scipal, K.; Bonekamp, H.; Figa, J.; Anderson, C. Initial soil moisture retrievals from the METOP—A Advanced Scatterometer (ASCAT). *Geophys. Res. Lett.* **2007**, *34*, L20401. [CrossRef]
165. Liu, Y.; Zha, Y.; Ran, G.; Zhang, Y.; Shi, L. SMRFR: A global multilayer soil moisture dataset generated using Random Forest from multi-source data. *Sci. Data* **2025**, *12*, 1170. [CrossRef]
166. Dorigo, W.; Wagner, W.; Albergel, C.; Albrecht, F.; Balsamo, G.; Brocca, L.; Chung, D.; Ertl, M.; Forkel, M.; Gruber, A.; et al. ESA CCI Soil Moisture for improved Earth system understanding: State-of-the art and future directions. *Remote Sens. Environ.* **2017**, *203*, 185–215. [CrossRef]
167. Jiang, H.; Shen, H.; Li, X.; Li, L. *The 43-Year (1978–2020) Global 9 Km Remotel y Sensed Soil Moisture Product [dataset]*; PANGAEA: Bremen, Germany, 2022. [CrossRef]
168. Ling, X.; Huang, Y.; Guo, W.; Wang, Y.; Chen, C.; Qiu, B.; Ge, J.; Qin, K.; Xue, Y.; Peng, J. Comprehensive evaluation of satellite-based and reanalysis soil moisture products using in situ observations over China. *Hydrol. Earth Syst. Sci.* **2021**, *25*, 4209–4229. [CrossRef]
169. Yufang, Z.; Shunlin, L.; Han, M.; Tao, H.; Qian, W.; Bing, L.; Jianglei, X.; Guodong, Z.; Xiaobang, L.; Changhao, X. Generation of global 1 km daily soil moisture product from 2000 to 2020 using ensemble learning. *Earth Syst. Sci. Data* **2023**, *15*, 2055–2079. [CrossRef]
170. Zheng, J.; Zhao, T.; Lü, H.; Shi, J.; Cosh, M.H.; Ji, D.; Jiang, L.; Cui, Q.; Lu, H.; Yang, K.; et al. Assessment of 24 soil moisture datasets using a new in situ network in the Shandian River Basin of China. *Remote Sens. Environ.* **2022**, *271*, 112891. [CrossRef]
171. Kang, C.S.; Zhao, T.; Shi, J.; Cosh, M.H.; Chen, Y.; Starks, P.J.; Collins, C.H.; Wu, S.; Sun, R.; Zheng, J. Global Soil Moisture Retrievals from the Chinese FY-3D Microwave Radiation Imager. *IEEE Trans. Geosci. Remote Sens.* **2021**, *59*, 4018–4032. [CrossRef]
172. Reichle, R.H.; Draper, C.S.; Liu, Q.; Girotto, M.; Mahanama, S.P.P.; Koster, R.D.; De Lannoy, G.J.M. Assessment of MERRA-2 Land Surface Hydrology Estimates. *J. Clim.* **2017**, *30*, 2937–2960. [CrossRef]
173. Gelaro, R.; Mccarty, W.; Suárez, M.J.; Todling, R.; Molod, A.; Takacs, L.; Randles, C.A.; Darmenov, A.; Bosilovich, M.G.; Reichle, R.; et al. The Modern-Era Retrospective Analysis for Research and Applications, Version 2 (MERRA-2). *J. Clim.* **2017**, *30*, 5419–5454. [CrossRef]
174. Koster, R.D.; Suarez, M.J. Technical Report Series on Global Modeling and Data Assimilation. *NASA Tech. Memo.* **1996**, *9*, 104606.
175. Beaudoing, H.; Rodell, M. *GLDAS Noah Land Surface Model L4 3 Hourly 0.25 x 0.25 Degree, Version 2.1*; The NASA Goddard Earth Science Data and Information Services Center: Greenbelt, MD, USA, 2020. [CrossRef]
176. Geng, M.; Zhang, F.; Chang, X.; Wu, Q.; Liang, L. Spatial-temporal Variation of Soil Moisture in China from Long Time Series Based on GLDAS-Noah. *Sens. Mater.* **2021**, *33*, 4643–4658. [CrossRef]
177. Miralles, D.G.; De Jeu, R.A.M.; Gash, J.H.; Holmes, T.R.H.; Dolman, A.J. An application of GLEAM to estimating global evaporation. *Hydrol. Earth System. Sci. Discuss.* **2011**, *8*, 1–27. [CrossRef]
178. Hulsman, P.; Keune, J.; Koppa, A.; Schellekens, J.; Miralles, D.G. Incorporating Plant Access to Groundwater in Existing Global, Satellite-Based Evaporation Estimates. *Water Resour. Res.* **2023**, *59*, e2022WR033731. [CrossRef]
179. Yin, J.; Zhan, X.; Liu, J. NOAA Satellite Soil Moisture Operational Product System (SMOPS) Version 3.0 Generates Higher Accuracy Blended Satellite Soil Moisture. *Remote Sens.* **2020**, *12*, 2861. [CrossRef]
180. Liu, J.; Zhan, X.; Hain, C.; Yin, J.; Fang, L.; Li, Z.; Zhao, L. NOAA soil moisture operational product system (SMOPS) and its validations. In Proceedings of the 2016 IEEE International Geoscience and Remote Sensing Symposium (IGARSS), Beijing, China, 10–15 July 2016; pp. 3477–3480.
181. Vergopolan, N.; Chaney, N.W.; Beck, H.E.; Pan, M.; Sheffield, J.; Chan, S.; Wood, E.F. Combining hyper-resolution land surface modeling with SMAP brightness temperatures to obtain 30-m soil moisture estimates. *Remote Sens. Environ.* **2020**, *242*, 111740. [CrossRef]
182. Sabater, J.M. ERA5-Land Hourly Data from 1950 to Present; Copernicus Climate Change Service (C3S) Climate Data Store (CDS). 2019. Available online: https://cds.climate.copernicus.eu/datasets/reanalysis-era5-land?tab=overview (accessed on 21 October 2025).
183. Fang, B.; Lakshmi, V.; Cosh, M.; Liu, P.W.; Bindlish, R.; Jackson, T.J. A global 1-km downscaled SMAP soil moisture product based on thermal inertia theory. *Vadose Zone J.* **2022**, *21*, e20182. [CrossRef]
184. Peng, Z.; Zhao, T.; Shi, J.; Hu, L.; Rodríguez-Fernández, N.J.; Wigneron, J.-P.; Jackson, T.J.; Walker, J.P.; Cosh, M.H.; Yang, K.; et al. First mapping of polarization-dependent vegetation optical depth and soil moisture from SMAP L-band radiometry. *Remote Sens. Environ.* **2024**, *302*, 113970. [CrossRef]

185. Kim, S.; Van Zyl, J.; Dunbar, R.; Njoku, E.; Johnson, J.; Moghaddam, M.; Tsang, L. *SMAP L3 Radar Global Daily 3 km EASE-Grid Soil Moisture, Version 2*; NASA National Snow and Ice Data Center Distributed Active Archive Center (NSIDC DAAC): Boulder, CO, USA, 2016. [CrossRef]
186. Jianting, H.; Na, Y.; Chao, M. Study on the Difference Characteristics between SMAP L2 Multiscale Soil Moisture Data and ISMN Filed Measurement. *Remote Sens. Technol. Appl.* **2022**, *37*, 1392–1403. Available online: http://www.rsta.ac.cn/EN/10.11873/j.issn.1004-0323.2022.6.1392 (accessed on 21 October 2025).
187. O'Neill, P.; Bindlish, R.; Chan, S.; Njoku, E.; Jackson, T. *Algorithm Theoretical Basis Document. Level 2 & 3 Soil Moisture (Passive) Data Products*; National Aeronautics and Space Administration (NASA): Washington, DC, USA, 2018.
188. Entekhabi, D.; Das, N.; Njoku, E.; Johnson, J.; Shi, J. *SMAP L3 Radar/Radiometer Global Daily 9 km EASE-Grid Soil Moisture, Version 2*; NASA National Snow and Ice Data Center Distributed Active Archive Center (NSIDC DAAC): Boulder, CO, USA, 2015.
189. Chen, Y.; Feng, X.; Fu, B. An improved global remote-sensing-based surface soil moisture (RSSSM) dataset covering 2003–2018. *Earth Syst. Sci. Data* **2021**, *13*, 1–31. [CrossRef]
190. Das, N.N.; Entekhabi, D.; Dunbar, R.S.; Chaubell, M.J.; Colliander, A.; Yueh, S.; Jagdhuber, T.; Chen, F.; Crow, W.; O'Neill, P.E.; et al. The SMAP and Copernicus Sentinel 1A/B microwave active-passive high resolution surface soil moisture product. *Remote Sens. Environ.* **2019**, *233*, 111380. [CrossRef]
191. Pablos, M.; Vall-llossera, M.; Piles, M.; Camps, A.; González-Haro, C.; Turiel, A. Influence of Quality Filtering Approaches in BEC SMOS L3 Soil Moisture Products. In Proceedings of the IGARSS 2019—2019 IEEE International Geoscience and Remote Sensing Symposium, Yokohama, Japan, 28 July–2 August 2019; pp. 6941–6944. [CrossRef]
192. Portabella, M. *SMOS L3 Surface Soil Moisture Binned Maps at 25 km EASE-2, Version 4.0*; CSIC–Instituto de Ciencias del Mar: Barcelona, Spain, 2022.
193. Spatafora, L.R.; Vall-llossera, M.; Camps, A.; Chaparro, D.; Alvalá, R.C.d.S.; Barbosa, H. Validation of SMOS L3 AND L4 Soil Moisture Products in the Remedhus (SPAIN) and Cemaden (BRAZIL) Networks. *Rev. Bras. Geogr. Fís.* **2020**, *13*, 691–712. [CrossRef]
194. Pablos, M.; González-Haro, C.; Portal, G.; Piles, M.; Vall-llossera, M.; Portabella, M. *SMOS L4 Surface Soil Moisture Downscaled Maps at 1 km EASE-2 (Reprocessed Mode), Version 6.1*; CSIC–Instituto de Ciencias del Mar: Barcelona, Spain, 2023.
195. Al Bitar, A.; Mialon, A.; Kerr, Y.H.; Cabot, F.; Richaume, P.; Jacquette, E.; Quesney, A.; Mahmoodi, A.; Tarot, S.; Parrens, M.; et al. The global SMOS Level 3 daily soil moisture and brightness temperature maps. *Earth Syst. Sci. Data* **2017**, *9*, 293–315. [CrossRef]
196. Keshavarz, R.; Shariati, N. High-Sensitivity and Compact Time Domain Soil Moisture Sensor Using Dispersive Phase Shifter for Complex Permittivity Measurement. *IEEE Trans. Instrum. Meas.* **2021**, *71*, 8001010. [CrossRef]
197. Abdelmoneim, A.A.; Khadra, R.; Derardja, B.; Dragonetti, G. Internet of Things (IoT) for Soil Moisture Tensiometer Automation. *Micromachines* **2023**, *14*, 236. [CrossRef]
198. Hamdany, A.H.; Shen, Y.; Satyanaga, A.; Rahardjo, H.; Lee, T.-T.D.; Nong, X. Field instrumentation for real-time measurement of soil-water characteristic curve. *Int. Soil. Water Conserv. Res.* **2022**, *10*, 586–596. [CrossRef]
199. Nandi, R.; Shrestha, D. Assessment of Low-Cost and Higher-End Soil Moisture Sensors across Various Moisture Ranges and Soil Textures. *Sensors* **2024**, *24*, 5886. [CrossRef] [PubMed]
200. Brogi, C.; Jakobi, J.; Huisman, J.A.; Schmidt, M.; Montzka, C.; Bates, J.S.; Akter, S.; Bogena, H.R. Cosmic-ray neutron sensors provide scale-appropriate soil water content and vegetation observations for eddy covariance stations in agricultural ecosystems. *Agric. For. Meteorol.* **2025**, *373*, 110731. [CrossRef]
201. Rasche, D.; Weimar, J.; Schrön, M.; Köhli, M.; Morgner, M.; Güntner, A.; Blume, T. A change in perspective: Downhole cosmic-ray neutron sensing for the estimation of soil moisture. *Hydrol. Earth Syst. Sci.* **2023**, *27*, 3059–3082. [CrossRef]
202. Qi, Q.; Yang, H.; Zhou, Q.; Han, X.; Jia, Z.; Jiang, Y.; Chen, Z.; Hou, L.; Mei, S. Performance of Soil Moisture Sensors at Different Salinity Levels: Comparative Analysis and Calibration. *Sensors* **2024**, *24*, 6323. [CrossRef]
203. Emamalizadeh, S.; Pirola, A.; Alessandrini, C.; Balenzano, A.; Baroni, G. Comparison of Soil Water Content from SCATSAR-SWI and Cosmic Ray Neutron Sensing at Four Agricultural Sites in Northern Italy: Insights from Spatial Variability and Representativeness. *Remote Sens.* **2024**, *16*, 3384. [CrossRef]
204. Chen, S.; Wen, Z.; Jiang, H.; Zhao, Q.; Zhang, X.; Chen, Y. Temperature Vegetation Dryness Index Estimation of Soil Moisture under Different Tree Species. *Sustainability* **2015**, *7*, 11401–11417. [CrossRef]
205. Liu, Z.; Zheng, J.; Zhu, Z.; Qu, Y.; Xu, Z. Applicability Research of Parameters in Soil Moisture Inversion. *Geogr. Sci. Res.* **2022**, *11*, 395–406. [CrossRef]
206. Zribi, M.; Muddu, S.; Bousbih, S.; Al Bitar, A.; Tomer, S.K.; Baghdadi, N.; Bandyopadhyay, S. Analysis of L-Band SAR Data for Soil Moisture Estimations over Agricultural Areas in the Tropics. *Remote Sens.* **2019**, *11*, 1122. [CrossRef]
207. Khabbazan, S.; Steele-Dunne, S.C.; Vermunt, P.; Judge, J.; Vreugdenhil, M.; Gao, G. The influence of surface canopy water on the relationship between L-band backscatter and biophysical variables in agricultural monitoring. *Remote Sens. Environ.* **2022**, *268*, 112789. [CrossRef]

208. Xu, N.; Daccache, A.; Ahmadi, A.; Houtz, D.; Perez-Barquero, F.P. Soil moisture estimation with microwave remote sensing: A systematic review and meta-analysis. *Int. J. Digit. Earth* **2025**, *18*, 1–27. [CrossRef]
209. Li, Y.-y.; Zhao, K.; Zheng, X.-m.; Ren, J.-h. Analysis of microwave polarization difference index characteristics about different vegetation types in northeast of China. In Proceedings of the 2013 the International Conference on Remote Sensing, Environment and Transportation Engineering (RSETE 2013), Nanjing, China, 26–28 July 2013; pp. 36–38. [CrossRef]
210. Zeng, J.; Peng, J.; Zhao, W.; Ma, C.; Ma, H. Microwave Remote Sensing of Soil Moisture. *Remote Sens.* **2023**, *15*, 4243. [CrossRef]
211. Silveira, J.M.d.C.; Góes, J.d.A.; Prado, D.F.S.; Pires, R.C.d.M.; Chiorato, A.F. Baselines for Calculating Crop Water Stress Index in Bean Cultivation. *Int. Arch. Photogramm. Remote Sens. Spat. Inf. Sci.* **2024**, *XLVIII-3-2024*, 501–506. [CrossRef]
212. Paloscia, S.; Pampaloni, P.; Santi, E. Radiometric Microwave Indices for Remote Sensing of Land Surfaces. *Remote Sens.* **2018**, *10*, 1859. [CrossRef]
213. Singh, A.; Meena, G.K.; Kumar, S.; Gaurav, K. Analysis of the Effect of Incidence Angle and Moisture Content on the Penetration Depth of L- and S-Band Sar Signals into the Ground Surface. *ISPRS Ann. Photogramm. Remote Sens. Spat. Inf. Sci.* **2018**, *IV-5*, 197–202. [CrossRef]
214. Verhoest, N.E.; Lievens, H.; Wagner, W.; Alvarez-Mozos, J.; Moran, M.S.; Mattia, F. On the Soil Roughness Parameterization Problem in Soil Moisture Retrieval of Bare Surfaces from Synthetic Aperture Radar. *Sensors* **2008**, *8*, 4213. [CrossRef]
215. Zeng, J.; Chen, K.S.; Cui, C.; Bi, H. Development and Validation of a New Passive Microwave Based Soil Moisture Index. *ISPRS Ann. Photogramm. Remote Sens. Spat. Inf. Sci.* **2020**, *V-3-2020*, 125–131. [CrossRef]
216. Mohan, M.M.P.; Kanchirapuzha, R.; Varma, M.R.R. Review of approaches for the estimation of sensible heat flux in remote sensing-based evapotranspiration models. *J. Appl. Remote Sens.* **2020**, *14*, 041501. [CrossRef]
217. Wu, P.; Yin, Z.; Zeng, C.; Duan, S.-B.; Gottsche, F.-M.; Ma, X.; Li, X.; Yang, H.; Shen, H. Spatially Continuous and High-Resolution Land Surface Temperature Product Generation: A review of reconstruction and spatiotemporal fusion techniques. *IEEE Geosci. Remote Sens. Mag.* **2021**, *9*, 112–137. [CrossRef]
218. Rahman, M.M.; Zhang, W. Review on estimation methods of the Earth's surface energy balance components from ground and satellite measurements. *J. Earth Syst. Sci.* **2019**, *128*, 84. [CrossRef]
219. Wanner, L.; Jung, M.; Paleri, S.; Butterworth, B.J.; Desai, A.R.; Sühring, M.; Mauder, M. Towards Energy-Balance Closure with a Model of Dispersive Heat Fluxes. *Bound.-Layer. Meteorol.* **2024**, *190*, 25. [CrossRef]
220. Butterworth, B.J.; Desai, A.R.; Durden, D.; Kadum, H.; LaLuzerne, D.; Mauder, M.; Metzger, S.; Paleri, S.; Wanner, L. Characterizing energy balance closure over a heterogeneous ecosystem using multi-tower eddy covariance. *Front. Earth Sci.* **2024**, *11*, 1251138. [CrossRef]
221. Bastiaanssena, W.G.M.; Menentia, M.; Feddesb, R.A.; Holtslag, A.A.M. A remote sensing surface energy balance algorithm for land (SEBAL). *J. Hydrol.* **1998**, *212–213*, 198–212. [CrossRef]
222. Wang, J.; Luo, S.; Li, Z.; Wang, S.; Li, Z. The freeze/thaw process and the surface energy budget of the seasonally frozen ground in the source region of the Yellow River. *Theor. Appl. Climatol.* **2019**, *138*, 1631–1646. [CrossRef]
223. Luo, S.; Wang, J.; Pomeroy, J.W.; Lyu, S. Freeze–Thaw Changes of Seasonally Frozen Ground on the Tibetan Plateau from 1960 to 2014. *J. Clim.* **2020**, *33*, 9427–9446. [CrossRef]
224. De Matthaeis, P.; Le Vine, D.M.; Soldo, Y.; Llorente, A. Study of a Strong RFI Source at L-Band Using SMAP Radiometer Data. In Proceedings of the 2021 IEEE International Geoscience and Remote Sensing Symposium IGARSS, Brussels, Belgium, 11–16 July 2021; pp. 2048–2050.
225. Feldman, A.F.; Chaparro, D.; Entekhabi, D. Error Propagation in Microwave Soil Moisture and Vegetation Optical Depth Retrievals. *IEEE J. Sel. Top. Appl. Earth Obs. Remote Sens.* **2021**, *14*, 11311–11323. [CrossRef] [PubMed]
226. Ziółkowski, D.; Jakubiak, S. The Influence of Texture on Soil Moisture Modeling for Soils of Diverse Roughness Using Backscattering Coefficient and Polarimetric Decompositions Derived from Sentinel-1 Data. *Remote Sens.* **2025**, *17*, 3282. [CrossRef]
227. Brakhasi, F.; Walker, J.P.; Judge, J.; Liu, P.-W.; Shen, X.; Ye, N.; Wu, X.; Yeo, I.-Y.; Kim, E.; Kerr, Y.; et al. Soil moisture profile estimation under bare and vegetated soils using combined L-band and P-band radiometer observations: An incoherent modeling approach. *Remote Sens. Environ.* **2024**, *307*, 114148. [CrossRef]
228. Huang, S.; Zhang, X.; Chen, N.; Ma, H.; Fu, P.; Dong, J.; Gu, X.; Nam, W.H.; Xu, L.; Rab, G.; et al. A Novel Fusion Method for Generating Surface Soil Moisture Data with High Accuracy, High Spatial Resolution, and High Spatio-Temporal Continuity. *Water Resour. Res.* **2022**, *58*, e2021WR030827. [CrossRef]
229. Batchu, V.; Nearing, G.; Gulshan, V. A Deep Learning Data Fusion Model Using Sentinel-1/2, SoilGrids, SMAP, and GLDAS for Soil Moisture Retrieval. *J. Hydrometeorol.* **2023**, *24*, 1789–1823. [CrossRef]
230. Yi, C.; Li, X.; Xing, Z.; Xin, X.; Ren, Y.; Zhou, H.; Zhou, W.; Zhang, P.; Wu, T.; Wigneron, J.-P. An Assessment of the Seasonal Uncertainty of Microwave L-Band Satellite Soil Moisture Products in Jiangsu Province, China. *Remote Sens.* **2024**, *16*, 4235. [CrossRef]
231. Zhang, P.; Yu, H.; Gao, Y.; Zhang, Q. Evaluation of Remote Sensing and Reanalysis Products for Global Soil Moisture Characteristics. *Sustainability* **2023**, *15*, 9112. [CrossRef]

232. Madelon, R.; Rodríguez-Fernández, N.J.; Bazzi, H.; Baghdadi, N.; Albergel, C.; Dorigo, W.; Zribi, M. Soil moisture estimates at 1 km resolution making a synergistic use of Sentinel data. *Hydrol. Earth Syst. Sci.* **2023**, *27*, 1221–1242. [CrossRef]
233. Yang, Y.; Zhang, J.; Bao, Z.; Ao, T.; Wang, G.; Wu, H.; Wang, J. Evaluation of Multi-Source Soil Moisture Datasets over Central and Eastern Agricultural Area of China Using In Situ Monitoring Network. *Remote Sens.* **2021**, *13*, 1175. [CrossRef]
234. Rao, P.; Wang, Y.; Wang, F.; Liu, Y.; Wang, X.; Wang, Z. Daily soil moisture mapping at 1 km resolution based on SMAP data for desertification areas in northern China. *Earth Syst. Sci. Data* **2022**, *14*, 3053–3073. [CrossRef]
235. Sang, Y.; Ren, H.-L.; Li, M. Climatological Evaluation of Three Assimilation and Reanalysis Datasets on Soil Moisture over the Tibetan Plateau. *Remote Sens.* **2024**, *16*, 4198. [CrossRef]
236. Zheng, Y.; Coxon, G.; Woods, R.; Power, D.; Rico-Ramirez, M.A.; McJannet, D.; Rosolem, R.; Li, J.; Feng, P. Evaluation of reanalysis soil moisture products using cosmic ray neutron sensor observations across the globe. *Hydrol. Earth Syst. Sci.* **2024**, *28*, 1999–2022. [CrossRef]
237. Chapman, B.; Rosen, P. Overview of NASAS calibration and validation activities for the NISAR mission. In Proceedings of the EUSAR 2024; 15th European Conference on Synthetic Aperture Radar, Munich, Germany, 23–26 April 2024; pp. 1101–1103.
238. Davidson, M.; Gebert, N.; Giulicchi, L. ROSE-L—The L-band SAR Mission for Copernicus. In Proceedings of the EUSAR 2021; 13th European Conference on Synthetic Aperture Radar, Online, 29 March–1 April 2021; pp. 236–237.
239. Aniruddha, C. Technical Overview of ISRO and NASA's First Joint Mission: NASA-ISRO Synthetic Aperture Radar (NISAR) Satellite. *Acceleron Aerosp. J.* **2024**, *3*, 563–572. [CrossRef]
240. Pierdicca, N.; Davidson, M.; Chini, M.; Dierking, W.; Djavidnia, S.; Haarpaintner, J.; Hajduch, G.; Laurin, G.; Lavalle, M.; López-Martínez, C.; et al. *The Copernicus L-Band SAR Mission ROSE-L (Radar Observing System for Europe) (Conference Presentation)*; SPIE: Strasbourg, France, 2019; Volume 11154.
241. Davidson, M.; Kubanek, J.; Iannini, L.; Furnell, R.; Di Cosimo, G.; Gebert, N.; Petrolati, D.; Geudtner, D.; Osborne, S. Rose-L—The Copernicus L-Band Synthetic Aperture Radar Imaging Mission. In Proceedings of the IGARSS 2023—2023 IEEE International Geoscience and Remote Sensing Symposium, Pasadena, CA, USA, 16–21 July 2023; pp. 4568–4571.
242. Yin, G.; He, W.; Liu, X.; Xia, Y.; Zhang, H. Wetting or greening? Probing the global trends in Vegetation Condition Index (VCI). *Int. J. Appl. Earth Obs. Geoinf.* **2024**, *129*, 103822. [CrossRef]
243. Zhang, T.; Yang, L.; Nan, H.; Yin, C.; Sun, B.; Yang, D.; Hong, X.; Lopez-Baeza, E. In-Situ GNSS-R and Radiometer Fusion Soil Moisture Retrieval Model Based on LSTM. *Remote Sens.* **2023**, *15*, 2693. [CrossRef]
244. Singh, A.; Gaurav, K. Deep learning and data fusion to estimate surface soil moisture from multi-sensor satellite images. *Sci. Rep.* **2023**, *13*, 2251. [CrossRef]
245. Li, S.; Zhu, P.; Song, N.; Li, C.; Wang, J. Regional Soil Moisture Estimation Leveraging Multi-Source Data Fusion and Automated Machine Learning. *Remote Sens.* **2025**, *17*, 837. [CrossRef]
246. Singh, A.; Gaurav, K. PIML-SM: Physics-Informed Machine Learning to Estimate Surface Soil Moisture from Multisensor Satellite Images by Leveraging Swarm Intelligence. *IEEE Trans. Geosci. Remote Sens.* **2024**, *62*, 4416913. [CrossRef]
247. Zheng, D.; Wang, X.; van der Velde, R.; Ferrazzoli, P.; Wen, J.; Wang, Z.; Schwank, M.; Colliander, A.; Bindlish, R.; Su, Z. Impact of surface roughness, vegetation opacity and soil permittivity on L-band microwave emission and soil moisture retrieval in the third pole environment. *Remote Sens. Environ.* **2018**, *209*, 633–647. [CrossRef]
248. Munoz-Martin, J.F.; Rodriguez-Alvarez, N.; Bosch-Lluis, X.; Oudrhiri, K. Effective Surface Roughness Impact in Polarimetric GNSS-R Soil Moisture Retrievals. *Remote Sens.* **2023**, *15*, 2013. [CrossRef]

Disclaimer/Publisher's Note: The statements, opinions and data contained in all publications are solely those of the individual author(s) and contributor(s) and not of MDPI and/or the editor(s). MDPI and/or the editor(s) disclaim responsibility for any injury to people or property resulting from any ideas, methods, instructions or products referred to in the content.